J Chem Biol (2011) 4:117–136
DOI 10.1007/s12154-011-0056-8

ORIGINAL ARTICLE

A new approach to the molecular analysis of docking, priming, and regulated membrane fusion

Tatiana P. Rogasevskaia · Jens R. Coorssen

Received: 14 October 2010 / Accepted: 23 December 2010 / Published online: 8 February 2011

Abstract Studies using isolated sea urchin cortical vesicles have proven invaluable in dissecting mechanisms of Ca^{2+}-triggered membrane fusion. However, only acute molecular manipulations are possible in vitro. Here, using selective pharmacological manipulations of sea urchin eggs ex vivo, we test the hypothesis that specific lipidic components of the membrane matrix selectively affect defined late stages of exocytosis, particularly the Ca^{2+}-triggered steps of fast membrane fusion. Egg treatments with cholesterol-lowering drugs resulted in the inhibition of vesicle fusion. Exogenous cholesterol recovered fusion extent and efficiency in cholesterol-depleted membranes; α-tocopherol, a structurally dissimilar curvature analogue, selectively restored fusion extent. Inhibition of phospholipase C reduced vesicle phosphatidylethanolamine and suppressed both the extent and kinetics of fusion. Although phosphatidylinositol-3-kinase inhibition altered levels of polyphosphoinositide species and reduced all fusion parameters, sequestering polyphosphoinositides selectively inhibited fusion kinetics. Thus, cholesterol and phosphatidylethanolamine play direct roles in the fusion pathway, contributing negative curvature. Cholesterol also organizes the physiological fusion site, defining fusion efficiency. A selective influence of phosphatidylethanolamine on fusion kinetics sheds light on the local microdomain structure at the site of docking/fusion. Polyphosphoinositides have modulatory upstream roles in priming: alterations in specific polyphosphoinositides likely represent the terminal priming steps defining fully docked, release-ready vesicles. Thus, this pharmacological approach has the potential to be a robust high-throughput platform to identify molecular components of the physiological fusion machine critical to docking, priming, and triggered fusion.

Keywords Sea urchin eggs · Cortical vesicles · Ca^{2+}-triggered fusion · Priming · Cholesterol · Phosphatidylethanolamine · Polyphosphoinositides

Abbreviations

CSC	Cell surface complexes
CV	Cortical vesicles
FFM	Fundamental fusion mechanism
PFM	Physiological fusion machine
PM	Plasma membrane
HMG-CoA reductase	3-Hydroxy-3-methylglutaryl-coenzyme reductase
PI-3K	Phosphatidylinositol-3-kinase
PLC	Phospholipase C
Atst	Atorvastatin
Smst	Simvastatin
Zara	Zaragozic acid
LY29	LY 294002
LY30	LY 303511

J. R. Coorssen (✉)
Department of Molecular Physiology, School of Medicine, and Molecular Medicine Research Group, and Nanoscale Research Group, University of Western Sydney,
Locked Bag 1797,
Penrith South DC, NSW 1797, Australia
e-mail: j.coorssen@uws.edu.au

T. P. Rogasevskaia
Department of Physiology and Pharmacology,
University of Calgary,
183 HMR, 3330 Hospital Drive NW,
Calgary, AB T2N 4N1, Canada

Wrt	Wortmannin
CHOL	Cholesterol
αT	α-Tocopherol
PC	Phosphatidylcholine
PE	Phosphatidylethanolamine
PIP	Polyphosphoinositides
PI	Phosphatidylinositol

Introduction

For decades, sea urchin (*Strongylocentrotus purpuratus*) eggs have been a convenient eukaryotic system for fundamental research in the fields of molecular, cellular, and reproductive biology. This 'cell' type plays a central role in studies of membrane-associated events, including regulated exocytosis. Shearing yields cell surface complexes (CSC)—plasma membrane (PM) sheets with docked, fusion-ready cortical vesicles (CV), from which high purity CV are isolated [29, 31, 85, 96]. Unlike mammalian secretory vesicles, CV retain Ca^{2+} sensitivity and fusion competence in vitro hours after isolation—washed free of soluble components, CV are 'locked' in the docked, fusion-ready state, requiring only an increase in $[Ca^{2+}]_{free}$ to trigger fusion [30, 57, 75, 80, 90]. Being amenable to biochemical manipulations, CSC and CV have proven invaluable in dissecting molecular mechanisms underlying docking, Ca^{2+}-triggering, and membrane fusion; comparable quantitative manipulations are unfeasible in other secretory systems [30, 76, 97].

Although unfertilized eggs are considered 'metabolically sluggish', maintenance of cell integrity and readiness of molecular mechanisms, including triggered fusion, dictate that critical metabolic activities are on-going. Here we establish that selective pharmacological manipulations of sea urchin eggs ex vivo effect molecular changes critical to defined late stages of exocytosis. We use this system to test the hypothesis that specific lipidic components of the membrane matrix selectively affect the mechanisms underlying vesicle docking, priming, and particularly fast, Ca^{2+}-triggered membrane fusion. We used (a) simvastatin (Smst) and atorvastatin (Atst), inhibiting 3-hydroxy-3-methylglutaryl-coenzyme A (HMG-CoA) conversion to mevalonate in cholesterol (CHOL) biosynthesis [11, 45, 48]; (b) zaragozic acid (Zara), suppressing squalene synthase activity and thus farnesyl pyrophosphate conversion to squalene [6, 77]; (c) D609, inhibiting phosphatidylcholine (PC) hydrolysis to diacylglycerol by phospholipase C (PLC) [60]; and (d) wortmannin (Wrt) and LY294002 (LY29), inhibiting phosphatidylinositol-3-kinase (PI-3K) activity and hence phosphorylation of polyphosphoinositides (PIP) at the third hydroxyl group, altering production of phosphatidylinositol-3-phosphate (PI(3)P), phosphatidylinositol-(3,4)-bisphosphate (PI(3,4)P2), and phosphatidylinositol-(3,4,5)-trisphosphate (PI(3,4,5)P3) [91, 94]. Isolated CSC and/or CV were then quantitatively assessed for molecular alterations and effects on Ca^{2+}-triggered fusion. To assess PIP, we developed separation and detection protocols for automated, high performance thin layer chromatography (HPTLC) [24, 26, 72]. Cinnamycin and neomycin, having high affinity for phosphatidylethanolamine (PE) and PIP, respectively, were also used to block these species in order to further define lipid functions.

This integrated approach capitalizes on the metabolic activity of unfertilized sea urchin eggs to effect endogenous alterations of molecular components involved in docking, priming, and Ca^{2+}-triggered fusion; CHOL, PE, and PIP levels were altered via inhibition of synthesis rather than by physically disrupting membrane structure with reagents that remove these lipids from the membrane [26, 27]. This approach thus firmly establishes critical but also differing roles for CHOL and PE in membrane fusion and indicates modulatory roles for PIP—these are unlikely to act directly in membrane merger but specific species likely underlie the final priming steps in the docked state; depriming from this release-ready state does not, however, result in undocking of vesicles.

Materials and methods

Materials

S. purpuratus were purchased from Westwind Sea Laboratories (Victoria, BC, Canada). CHOL, phospholipid, neutral lipid, and PIP standards were from Avanti Polar Lipids (Alabaster, AL, USA). LY29, Smst, Zara, D609, hydroxypropyl-β-cyclodextrin (hpβcd), α-tocopherol (αT), A23187, molybdenum blue reagent, and neomycin were from Sigma-Aldrich (St. Louis, MO, USA). Atst was from Research Chemicals (Toronto, ON, Canada), Wrt from BIOMOL International (Plymouth Meeting, PA, USA), and LY 303511 (LY30) from Calbiochem (Darmstadt, Germany). Cinnamycin was a gift from Roche Pharmaceuticals (Switzerland). IPG strips and Sypro-Ruby stain were from Bio-Rad (Hercules, CA, USA). All other chemicals were of at least analytical grade.

Egg manipulations

Fresh sea urchin eggs were obtained by 0.5 M KCl intracoelomic injection and collected in artificial sea water [34]. The jelly coat was removed by passages through nylon mesh (100 μM pore size), followed by centrifugation (700×*g*). Pelleted eggs (5 ml) were suspended in 20 ml of Ca^{2+}-free artificial sea water (CFASW) [34] and incubated

at 7 °C for 20 h with continuous gentle mixing; Smst, Atst, Zara, D609, Wrt, LY29, and LY30 were added to suspensions at the start of the incubation. Atst, Smst, LY29, LY30, Wrt, and A23187 were delivered from dimethyl sulfoxide (DMSO) stocks (≤1% DMSO, final); Zara and D609 were delivered as high concentration aqueous solutions. To confirm preservation of native CV fusion following incubations (i.e., capacity to raise fertilization envelopes), intact eggs were transferred to room temperature for 60–120 s in CFASW, containing added Ca^{2+} (50 μM) and the ionophore A23187 (100 μM). Bright field images were acquired with a Zeiss microscope (Carl Zeiss Inc, Oberkochen, Germany) (neoflurar ×6.3/0.20 objective) equipped with an AxioCam camera and AxioVision software.

CSC and CV preparations, treatments, and fusion assays

CSC/CV were isolated from fresh and 20-h incubated eggs using standard protocols [27, 30, 31]. Acute treatments and fusion assays were carried out in baseline intracellular media (BIM—210 mM potassium glutamate, 500 mM glycine, 10 mM NaCl, 10 mM 1,4-piperazinediethanesulfonic acid (PIPES), 1 mM $MgCl_2$, 0.05 mM $CaCl_2$, 1 mM ethyleneglycoltetraacetic acid (EGTA); pH 6.7) with the addition of protease inhibitors and 2.5 mM adenosine triphosphate (ATP) [30]. Cinnamycin was delivered to CV suspensions (optical density $(OD)_{405}$ 0.4) from DMSO/BIM (1:9) stocks, while neomycin was delivered from an aqueous solution (OD_{405} 0.4). CV, isolated from fresh eggs, were treated with cinnamycin and neomycin for 30 min (25 °C) followed by fusion assays. For fusion recovery, CV suspensions (OD_{405} 1.0), isolated from Smst-/Atst-incubated eggs, were treated with 2 mM CHOL-loaded hpβcd or 200 μM αT for 30 min (25 °C), centrifuged, and suspended in fresh BIM for fusion assays; CHOL-loaded hpβcd was prepared as described [27, 42, 70]. αT was delivered in hexadecane (<0.1% solvent, final) [26, 27]. CV/CSC end-point and kinetic fusion assays and CV 'settle' fusion assays to assess inter-membrane attachment were as described [27, 31, 41, 87, 98]. Briefly, suspensions of free-floating CV were aliquoted into multi-well plates and low speed centrifugation was used to bring the CV gently into contact at the bottom of the wells. For the 'settle' fusion assay, aliquoted CV suspensions were simply allowed to settle into contact for 60 min before Ca^{2+} addition. OD measurements (initial suspension OD_{405}=0.4 for CV and OD_{405}=0.3 for CSC) were taken before and after the addition of various Ca^{2+} stocks, and the final $[Ca^{2+}]_{free}$ were measured with a Ca^{2+}-sensitive electrode (Nicossensors, Huntington Valley, PA, USA), as described [31]. All fusion measurements were carried out using a Victor^{2}V microplate-reader (Perkin Elmer, Boston, MA, USA). The data were normalized to the control conditions with the low and high $[Ca^{2+}]_{free}$ plateaus defining 0% and 100% fusion, respectively. The resulting Ca^{2+}–activity curves were fit using the sigmoidal cumulative log-normal model to establish fusion extent and Ca^{2+} sensitivity; the applicability of a log-normal cumulative distribution function to exocytotic survival and thus Ca^{2+}–activity curves has been clearly demonstrated [8, 49, 84]—the fraction of CV that fuse at a given $[Ca^{2+}]_{free}$ is solely a function of the average number of active fusion complexes (<*n*>) at a docking site. As CV–CV fusion proceeds through the same fusion complexes as exocytosis, it is fully described by the same analysis developed for CV–PM fusion, yielding comparable fitting parameters for the sigmoidal relationship between <*n*> and $[Ca^{2+}]_{free}$ [8, 27, 31, 84]. Curves for controls were thus fit to a two-parameter model with 100% fusion extent, and curves for treated conditions were fit to a three-parameter model (TableCurve-2D, v.5.0, SYSTAT, Richmond, CA, USA). Initial kinetics were fit with a linear equation over the first 0.5 s (i.e., injection time) [27]. Each condition was tested in four to eight replicates per experiment. Each experiment was repeated as indicated (*n*). Free-floating CV in suspension were counted using a hemocytometer [35].

Lipid extraction and HPTLC

CV (OD_{405} 0.4) membranes were isolated as described [26], and lipids extracted with methanol/chloroform [9]. For PIP, the extraction procedure was modified [68]; to induce phase separation, chloroform addition was followed by 1.76% KCl, 100 mM citric acid, 100 mM Na_2HPO_4, and 5 mM EDTA (pH 3.6). After collecting the organic phase, 0.88% KCl was added to the aqueous phase, followed by extraction with water-saturated butanol. After 30 min on ice, this butanol-rich phase was combined with the initial organic phase. To minimize PIP losses, all glassware was silanized according to the manufacturer's instructions (Sigmacote, Sigma).

Dried lipid extracts were dissolved in 100 μl chloroform/methanol (2:1, *v*/*v*) and loaded (using LINOMAT IV, CAMAG, Switzerland) onto silica gel 60 HPTLC plates (EMD Chemicals, Darmstadt, Germany) with a parallel dilution series of standards. All standards were the oleic acid (18:1Δ9) esters. For neutral and phospholipid separations, plates were pre-washed with chloroform/ethyl acetate (6:4, *v*/*v*) and activated (110 °C; 30 min) [26, 27]. Phospholipids and lysophospholipids were resolved using a two-step separation: 90 mm with dichloromethane/ethyl acetate/acetone (80:16:4, *v*/*v*/*v*) and then 90 mm with chloroform/ethylacetate/acetone/isopropanol/ethanol/methanol/water/acetic acid (30:6:6:6:16:28:6:2, *v*/*v*/*v*/*v*/*v*/*v*/*v*/*v*) [24]. Neutral lipids were resolved in five steps: 40 and 55 mm with dichloromethane/ethyl acetate/acetone (80:16:4, *v*/*v*/*v*), then 68, 80, and 90 mm with hexane/ethyl

acetate (90:10, 95:5, and 100:0, *v*/*v*, respectively) using the CAMAG AMD2 multi-development HPTLC unit [24, 27]. For αT analysis, samples were separated in four sequential steps: 30 mm with dichloromethane/ethyl acetate/acetone (80:16:4, *v*/*v*/*v*), then 50, 70, and 90 mm with 92:8, 95:5, and 98:2 (*v*/*v*) hexane/ethyl acetate, respectively [24]. For PIP resolution, plates were pre-washed with 1% (*w*/*v*) potassium oxalate (in methanol/water (2:3, *v*/*v*), 1 mM EDTA) for a few seconds and activated (110 °C, 30 min). PIP were resolved as described [50] but using a two-step development with the CAMAG AMD2; dichloromethane/ethyl acetate/acetone (80:16:4, *v*/*v*/*v*) was used to run neutral lipids to 90 mm, and then chloroform/methanol/ammonium hydroxide/water (57:50:4:11, *v*/*v*/*v*/*v*) was applied to 90 mm. This eliminated undesirable streaking on plates, yielding high resolution and reproducibility.

Cholesterol assay

CV membranes were isolated [24] and CHOL concentrations measured using the Amplex-Red CHOL assay kit (Invitrogen) according to the manufacturer's instructions.

Chromatogram visualization

For neutral lipids, phospholipids, and PI(4)P visualization, developed plates were exposed to 10% $CuSO_4$ in 8% H_3PO_4 aqueous solution, then charred as described [24, 72] and imaged (Ex 540 nm/Em 590 nm) with the PROXPRESS multi-wavelength fluorescent imager (Perkin Elmer). Integrated signal was compared to a parallel dilution series of standards on the same plate. All images were analyzed using ImageQuant5.2 (GE Healthcare, Piscataway, NJ, USA).

To quantify PIP in CV membrane extracts, a dilution series of PI, PI(4)P, PI(4,5)P2, PI(3,4)P2, PI(3,5)P2, and PI(3,4,5)P3 standards (Fig. 1a) were resolved in parallel with experimental samples. The PIP on-plate detection limit was defined as the minimal integrated fluorescence intensity of the lowest loaded quantity of standards detected after $CuSO_4$ staining; this fluorescence method showed limitations in detecting some PIP. The on-plate detection limit was ≥250 ng for PI(4,5)P2 and PI(3,4,5)P3 (corresponding to ≥1.71 and ≥1.57 amol/CV, respectively), and ≥500 ng for PI(3,4)P2 and PI(3,5)P2 (≥3.42 amol/CV) (Tables 1 and 2). In contrast, PI(4)P had a low on-plate detection limit of ≥50 ng (1.55 amol/CV), enabling routine, sensitive detection of this lipid. Levels of all CV PIP other than PI(4)P were thus well below detectable levels when using $CuSO_4$-based fluorescence detection. As an alternative, we tested molybdenum blue; using scanning densitometry (Fig. 1b), this reagent enabled routine detection of PI(3,4)P2 and PI(3,4,5)P3 in CV membranes. Briefly, plates were dipped into the reagent and then charred at 145 °C for 15 min; absorbance at 425 nm was then assessed using the CAMAG TLC2 scanner (CAMAG); this scanner was also used to quantify αT (characteristic absorbance of 288 nm) [26]. On-plate detection limits for PI(3,4)P2, PI(3,5)P2, and PI(3,4,5)P3 corresponded to ≥1.03, ≥1.03, and ≥0.94 amol/CV, respectively (Table 2, Fig. 10b), using standardized CV membrane extracts. On-plate detection limits for PI(4)P and PI(4,5)P2 standards corresponded to ≥1.84 and ≥1.71 amol/CV, respectively; thus, $CuSO_4$ charring was used for PI(4)P detection due to its higher sensitivity. Staining intensity with $CuSO_4$ and molybdenum blue did not correlate with the numbers of phosphate groups in PIP, but a phosphate at the third position of the inositol ring supported better molybdenum blue detection (Tables 1 and 2).

Membrane protein isolation and 2D gel electrophoresis

For protein extraction, CV were lysed with ice-cold PIPES buffer (20 mM PIPES, pH 7.0) supplemented with protease and phosphatase inhibitors [43]. Membranes were isolated by centrifugation (125,000×*g*, 4 °C, 3 h) and pellets incubated in chaotropic PKME buffer (425 mM KCl,

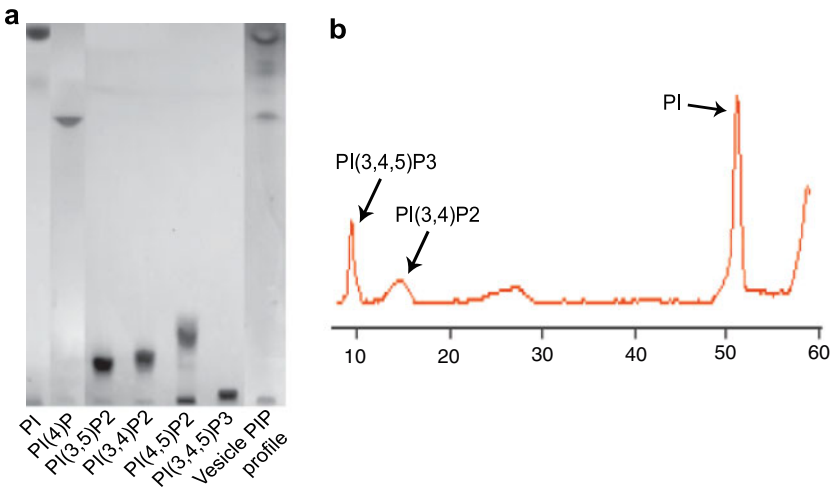

Fig. 1 Detection of phosphoinositides. **a** PIP standards assayed by HPTLC and $CuSO_4$ visualization method. **b** PIP detection by HPTLC and molybdenum blue method coupled with scanning densitometry. The trace shown is from a scanned TLC plate and representative of 11 such analyses

Table 1 On-plate detection of PIP standards

PIP species	On-plate detection limit	
	$CuSO_4$ charring (ng)	Molybdenum blue staining (ng)
PI(4)P	≥50	≥250
PI(4,5)P2	≥250	≥250
PI(3,4,5)P3	≥250	≥150
PI(3,4)P2	≥500	≥150
PI(3,5)P2	≥500	≥150

Table 2 On-plate detection of CV PIP species

PIP species	Amount detected per untreated CV (amol/CV)	
	$CuSO_4$ charring	Molybdenum blue staining
PI(4)P	1.55±0.08	≪1.84[a]
PI(4,5)P2	≪1.71[a]	≪1.71[a]
PI(3,4,5)P3	≪1.57[a]	1.22±0.08
PI(3,4)P2	≪3.42[a]	2.86±0.25
PI(3,5)P2	≪3.42[a]	≪1.03[a]

[a] CV samples below on-plate detection limit

10 mM $MgCl_2$, 5 mM EGTA, 50 mM PIPES, pH 6.7; with protease inhibitors), diluted with equivalent volumes of 2× BIM and centrifuged (125,000×*g*, 4 °C, 3 h). Pellets were solubilized in 2D sample buffer 4% CHAPS, 8 M urea, 2 M thiourea, protease, and phosphatase inhibitors; [12, 13] and protein concentrations were assayed using the EZ-Q protein quantification kit (Invitrogen). Sample reduction, alkylation, rehydration, isoelectric focusing, equilibration, and SDS-PAGE were carried out as described [12]. Linear 7-cm pH 3–10 IPG strips (Bio-Rad) were used for first dimension separations, and 20-cm second dimension separations were by 10–15% gradient PAGE.

Gel staining and image analysis

Gels were stained with Sypro-Ruby and imaged with the PROXPRESS system as described [12, 13]. Delta2D software (Decodon, Greifswald, Germany) was used for quantitative image analysis; average gel images were created using embedded automated analysis protocols. To ensure quantitative image analyses, we (1) consistently loaded the same amount of total proteins (100 μg) prior to first dimension separation, (2) integrated the Sypro-Ruby fluorescence for all samples to the same total intensity, and (3) normalized images to the total fluorescence volume [13]. Each sample was analyzed using three independent preparations and 2D gel separations.

Informatics

Sequence analyses of human and sea urchin enzymes were performed with BlastProtein (National Center for Biotechnology Information, USA) and sequence analyses of functional domains with ExPASy:ScanProsite (Swiss Institute of Bioinformatics, Switzerland).

Statistical analysis

All data are presented as mean ± SEM. Two-sample two-tailed *t* tests were used to assess differences between controls and experimental conditions. $P<0.05$ or $P<0.01$ was used to indicate statistical significance.

Results

To assess egg functional status after 20-h incubations at 7 °C, fresh and incubated eggs were compared. The following parameters were analyzed: (1) ability to raise fertilization envelopes upon Ca^{2+} influx (native exocytosis); (2) triggered CV–PM fusion in CSC preparations (exocytosis in vitro); (3) triggered CV–CV fusion in vitro; and (4) the CV membrane proteome and (5) lipidome. Fresh and incubated eggs formed fertilization envelopes equally well when challenged with Ca^{2+} and Ca^{2+}-ionophore (Fig. 2d, e). Thus, CV remained fully docked and fusion competent in intact eggs during incubations. CV–CV and CSC fusion reactions (Fig. 2a–c) showed no evidence that incubations had any effect on fusion, consistent with exocytosis assessments in intact eggs (Fig. 2d, e). CV–CV fusion had an EC_{50} of 20.6±1.0 μM $[Ca^{2+}]_{free}$ (Fig. 2a), and initial fusion rate was 73.8±2.6%/s, comparable to freshly isolated CV [26, 27, 38, 72]. Settle CV–CV fusion assays revealed no differences between fresh and incubated eggs, indicating that CV were able to form critical inter-membrane attachments necessary for a robust fusion response (Fig. 2b). The Ca^{2+} concentration required to trigger half maximal fusion in the 'settle' CV–CV fusion assay (EC_{50} of 30.8±0.7 μM $[Ca^{2+}]_{free}$, Fig. 2b) was only slightly higher than the Ca^{2+} sensitivity of homotypic CV–CV fusion (EC_{50} of 20.6±1.0 μM $[Ca^{2+}]_{free}$), but quite similar to the Ca^{2+} sensitivity of exocytosis in intact planar cortices (CV–PM fusion, EC_{50} of 30.4±0.7 μM $[Ca^{2+}]_{free}$; Fig. 2c), consistent with other studies [8, 26, 27, 31, 38, 39, 72, 84, 97]. Overlapping activity curves and kinetic responses found for both CV–CV and CV–PM fusion (Fig. 2) again suggested that the molecular machinery involved in the overall fusion process performed the same work in overcoming the fusion energy barrier [8, 31, 84]. Robust consistency of these curve-shaped parameters and thus translational invariance of the classic sigmoidal Ca^{2+}–

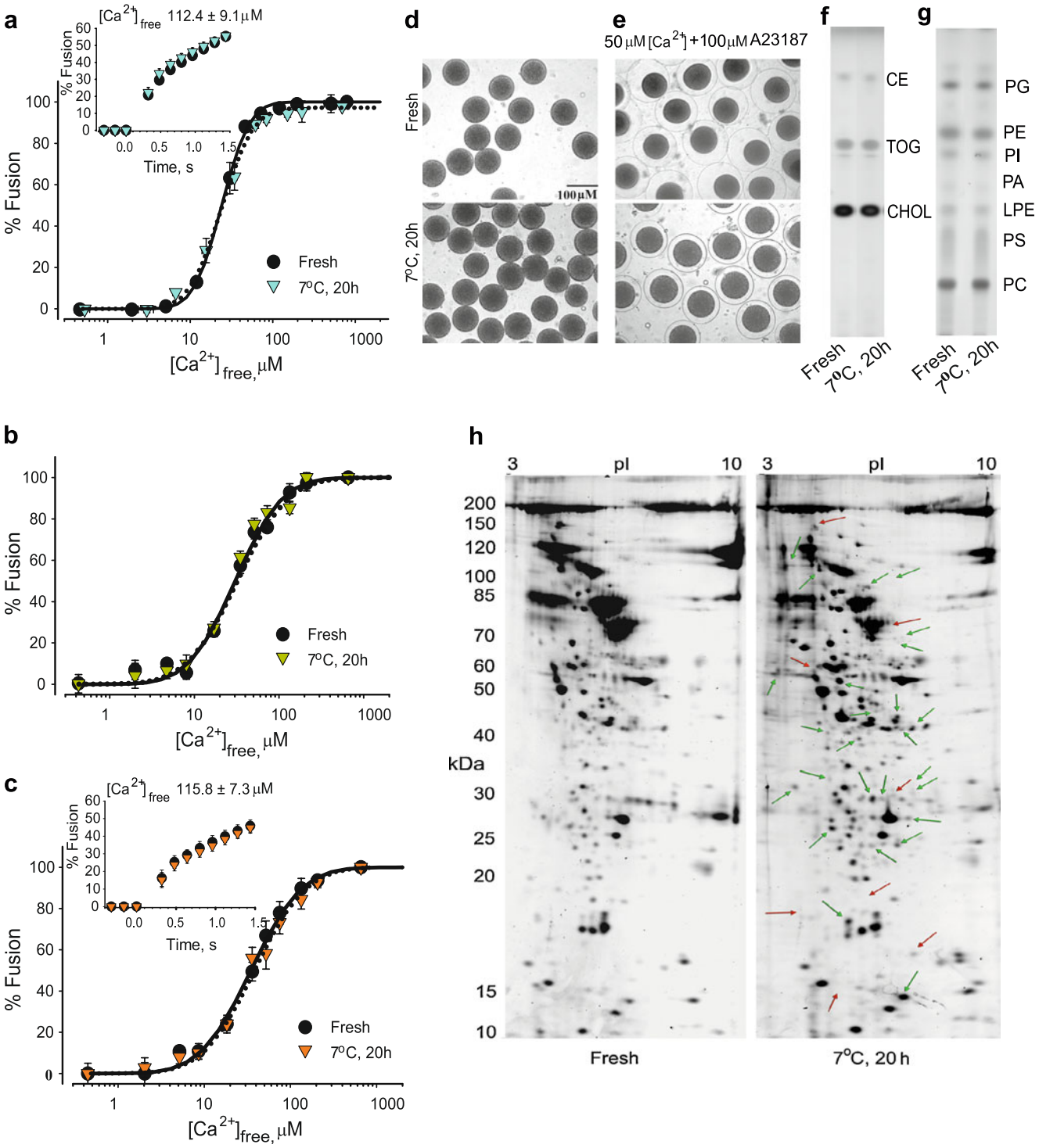

Fig. 2 Comparison of fresh and 20-h incubated preparations. **a** Ca^{2+}–activity curves for CV–CV fusion, including kinetics (*inset*) (n=5) (for CV isolated from fresh and incubated eggs). **b** Ca^{2+}–activity curves for 'settle' CV–CV fusion (n=5). **c** Ca^{2+}–activity curves for CSC fusion, including kinetics (*inset*) (n=4–5). **d** Fresh and incubated (7 °C) sea urchin eggs. **e** Fresh and incubated eggs after treatment with 50 μM Ca^{2+} and 100 μM A23187. Detection of **f** neutral and **g** phospholipids and lysolipids (representative of four separate experiments). Locations of lipid names correspond to co-resolved standards. *CHOL* cholesterol, *TOG* trioleoylglycerol, *CE* cholesterol esters, *PC* phosphatidylcholine, *LPA* lysophosphatidic acid, *PS* phosphatidylserine, *LPE* lysophosphatidylethanolamine, *PA* phosphatidic acid, *PI* phosphatidylinositol, *PE* phosphatidylethanolamine, *PG* phosphatidylglycerol. **h** 2D gel maps of CV membrane proteins isolated from fresh and incubated eggs. Protein relative abundance differences of >5-fold are indicated: average gel images are from three independent 2D gel separations; *green* and *red arrows* represent, respectively, increases and decreases in protein amounts

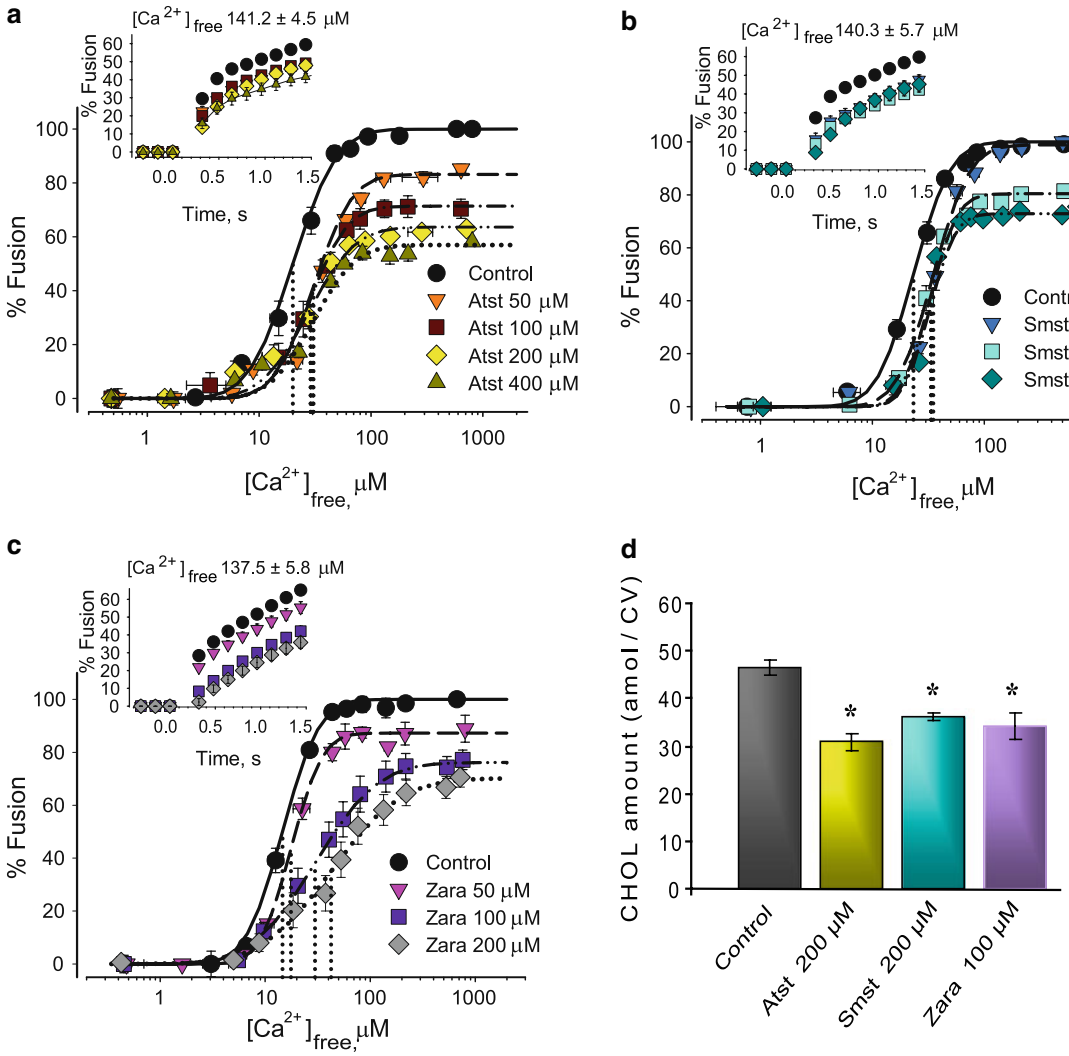

Fig. 3 CHOL-lowering agents inhibit CV–CV fusion. Ca^{2+}–activity curves of CV isolated from eggs incubated with **a** Atst (n=4–7), **b** Smst (n=5–7), and **c** Zara (n=3–4), including kinetics (*inset*). *Vertical dotted lines* indicate EC_{50} of each curve. **d** Quantification of CV membrane CHOL following incubations (n=4); *P<0.01 indicates significant difference from control

activity curves for both CV–CV and CV–PM fusion (Fig. 2) strongly indicates a common fusion mechanism, as might be anticipated of a vesicle that natively undergoes both hetero- and homotypic fusion [16].

Quantitative analyses revealed no significant differences in CV membrane lipid profiles (Fig. 2f, g), but alteration in the CV membrane proteins was observed. Proteome maps were compared by automated differential image analysis: 946±23 and 931±34 proteins were detected for CV from fresh and incubated eggs, respectively (Fig. 2h). We applied specific criteria to assess changes: (1) >5-fold differences in relative abundance were considered significant, and (2) alterations had to be 100% reproducible across a gel set [13]. Thirty-four proteins met these criteria, changing in relative abundance for incubated eggs. As these membrane proteome changes did not correlate with any alterations in fusion parameters and lipid profiles (Fig. 2), we were confident concerning the stability of critical molecular components; incubated eggs remained healthy and competent and could therefore be controls for pharmacological treatments.

Well-characterized acute CV manipulations identified multiple roles for CHOL in triggered fusion [25–27]. The correlation between decreased CV membrane CHOL and fusion inhibition was tested here by suppressing CHOL biosynthesis. Atst and Smst incubations resulted in a dose-dependent inhibition of fusion extent, Ca^{2+} sensitivity, and kinetics (Fig. 3a, b), correlating with reduced CHOL (Fig. 3d). CV from untreated eggs had 46.6±1.3 amol/CV of membrane CHOL, whereas CV from eggs treated with 200 μM Atst or Smst had significantly less CHOL—30.8±1.6 and 36.1±0.8 amol/CV, respectively—correlating with reductions in fusion extent (31.7±4.0% and 20.3±2.7%, respectively). For all Atst and Smst concentrations, the EC_{50} for fusion right-shifted maximally to 31.6±1.7 μM

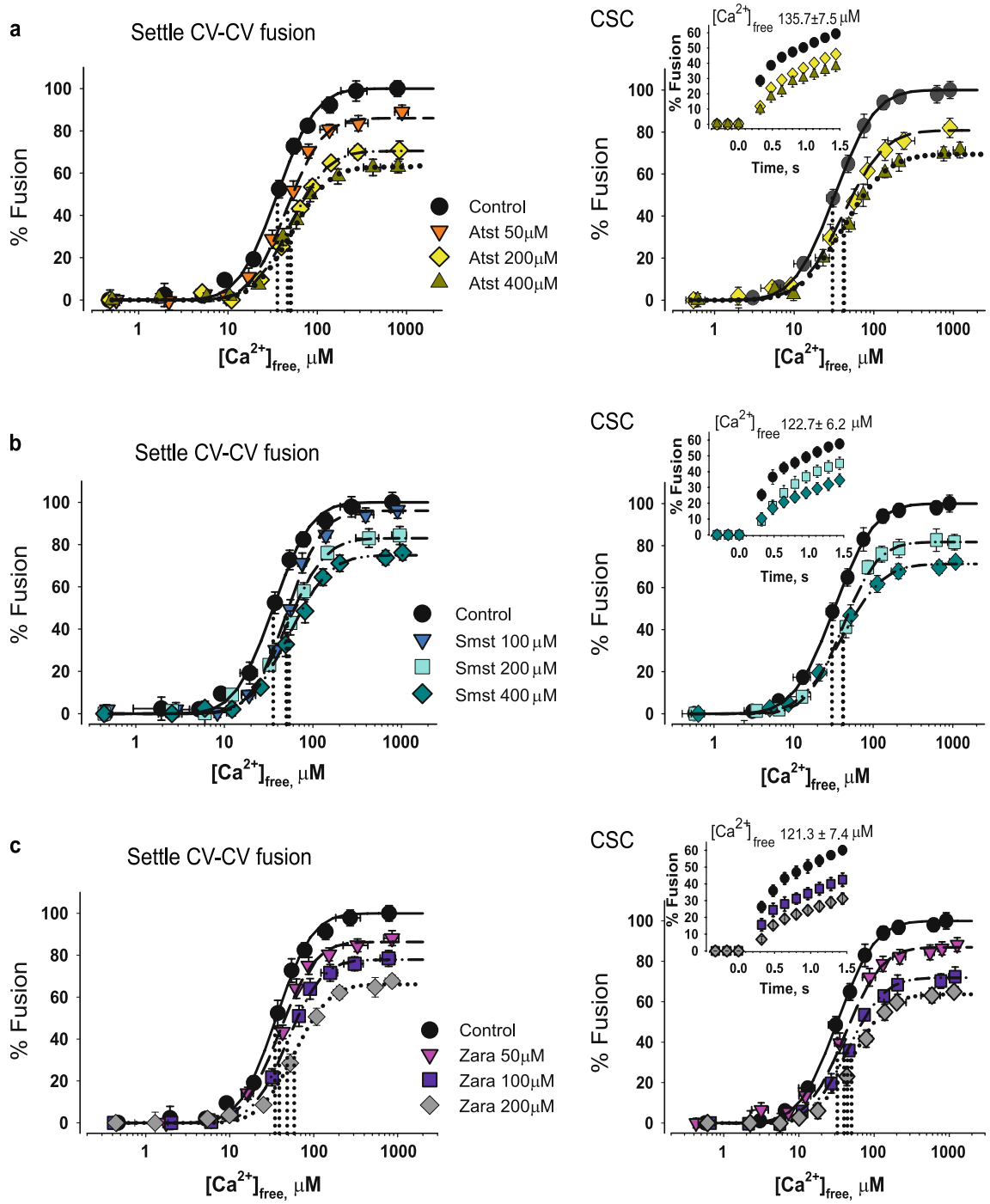

Fig. 4 CHOL-lowering agents inhibit CV–PM and settle CV–CV fusion. Ca^{2+}–activity curves of CV and CSC isolated from eggs incubated with **a** Atst (n=3–5), **b** Smst (n=3–4), and **c** Zara (n=3–5), including kinetics (*inset*). *Vertical dotted lines* indicate EC_{50} of each curve

$[Ca^{2+}]_{free}$ from control EC_{50} (20.6±1.0 μM $[Ca^{2+}]_{free}$) (Fig. 3a, b). Initial fusion rate (73.8±2.6%/s) decreased to 51.5±1.4%/s and 46.9±1.9%/s following 200 μM Atst or Smst, respectively. Atst caused potent inhibition of all fusion parameters, while inhibition of fusion extent by Smst saturated at lower concentrations; 100 μM Zara reduced the CHOL level from 46.6±1.3 to 34.1±2.7 amol/CV, comparable to Atst and Smst treatments (200 μM; Fig. 3d). This correlated with a decrease in fusion extent (by 23.3±6.6%), rightward shift in Ca^{2+} sensitivity (to EC_{50} 30.8±1.9 μM $[Ca^{2+}]_{free}$ vs. 20.6±1.0 μM $[Ca^{2+}]_{free}$ for controls), and potent inhibition of kinetics (28.4±1.1%/s vs. 73.8±2.6%/s for controls) (Fig. 3c). Atst, Smst, or Zara treatments did not affect other lipids (not shown). Notably, 200 μM Zara also caused a

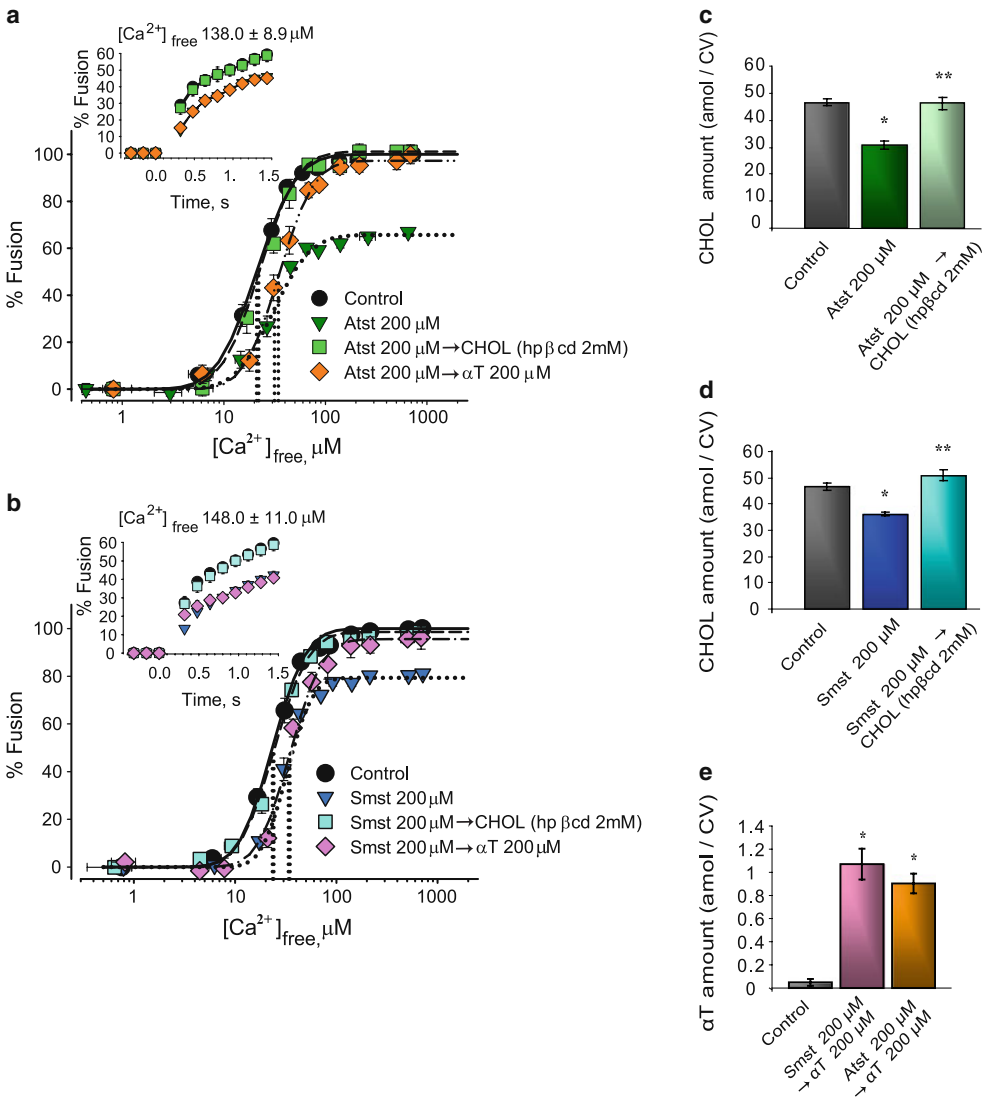

Fig. 5 Rescuing fusion in CHOL-depleted CV with exogenous CHOL (CHOL-loaded hpβcd) or αT. Ca^{2+}–activity curves for CV from eggs incubated with **a** Atst and **b** Smst and after subsequent supplementation with CHOL or αT, including kinetics (*inset*) (n=4). *Vertical dotted lines* indicate EC_{50} of each curve. Quantification of CV membrane CHOL following incubations with **c** Atst and **d** Smst and subsequent CHOL loading (n=4). **e** Quantification of CV membrane αT after Atst or Smst treatments and subsequent αT loading (n=4); *P<0.01, **P<0.01 indicate significant difference from control and other conditions, respectively

progressive rightward shift in Ca^{2+} sensitivity (to EC_{50} 42.5± 1.7 µM $[Ca^{2+}]_{free}$). CSC and settle CV–CV fusion assays confirmed these inhibitory effects on Ca^{2+}-triggered fusion and the correlation with decreased CHOL (Fig. 4); as there was no effect on settle assays, docking was unaffected.

CV from Atst- and Smst-treated eggs fully recovered native CHOL levels (Fig. 5c, d) and all fusion parameters when supplemented with exogenous CHOL (Fig. 5a, b). In contrast, CV from treated eggs showed selective recovery of fusion extent when rescued with 200 µM αT—neither Ca^{2+} sensitivity nor kinetics recovered (Fig. 5a, b, e). Fusion extent was recovered by the addition of 0.97± 0.08 amol of αT per CV for Atst-treated eggs (n=4) and 1.17±0.13 amol per CV for Smst-treated eggs (n=4). Initial fusion rate following Smst treatments was also partially recovered (~10%/s) by αT.

Egg incubations with D609 yielded significant increases in levels of endogenous PC (41.3±1.9 amol/CV) and lysoPE (20.9±1.5 amol/CV) and a decrease in PE (18.6± 0.9 amol/CV) relative to controls (31.6±1.1, 11.9±1.5, and 27.4±2.5 amol/CV, respectively) (Fig. 6c); no other changes in CV lipids were evident. These lipid changes correlated with a loss of Ca^{2+} sensitivity (EC_{50} right-shifted from 17.4±1.8 to 30.3±2.1 µM $[Ca^{2+}]_{free}$), 23.1±1.4% inhibition of fusion extent (already saturated at the lowest D609 concentration), and 18.4±1.1%/s inhibition of initial fusion rate (Fig. 6a). Comparable effects were seen in CSC and settle CV–CV assays (Fig. 7a).

To test whether the inhibition seen might be due to decreased endogenous PE, CV and CSC were treated acutely with cinnamycin, which has a high affinity for PE (binding ratio of 1:1; binding constant K_o of ~10^7–10^8 M^{-1}), but three orders less affinity for lysoPE (K_o of ~10^4–10^5 M^{-1}) [55]. Cinnamycin caused 19.1±1.5% inhibition of fusion extent at all concentrations tested (Figs. 6b and 7b). This inhibition was similar to that observed after incubations with D609.

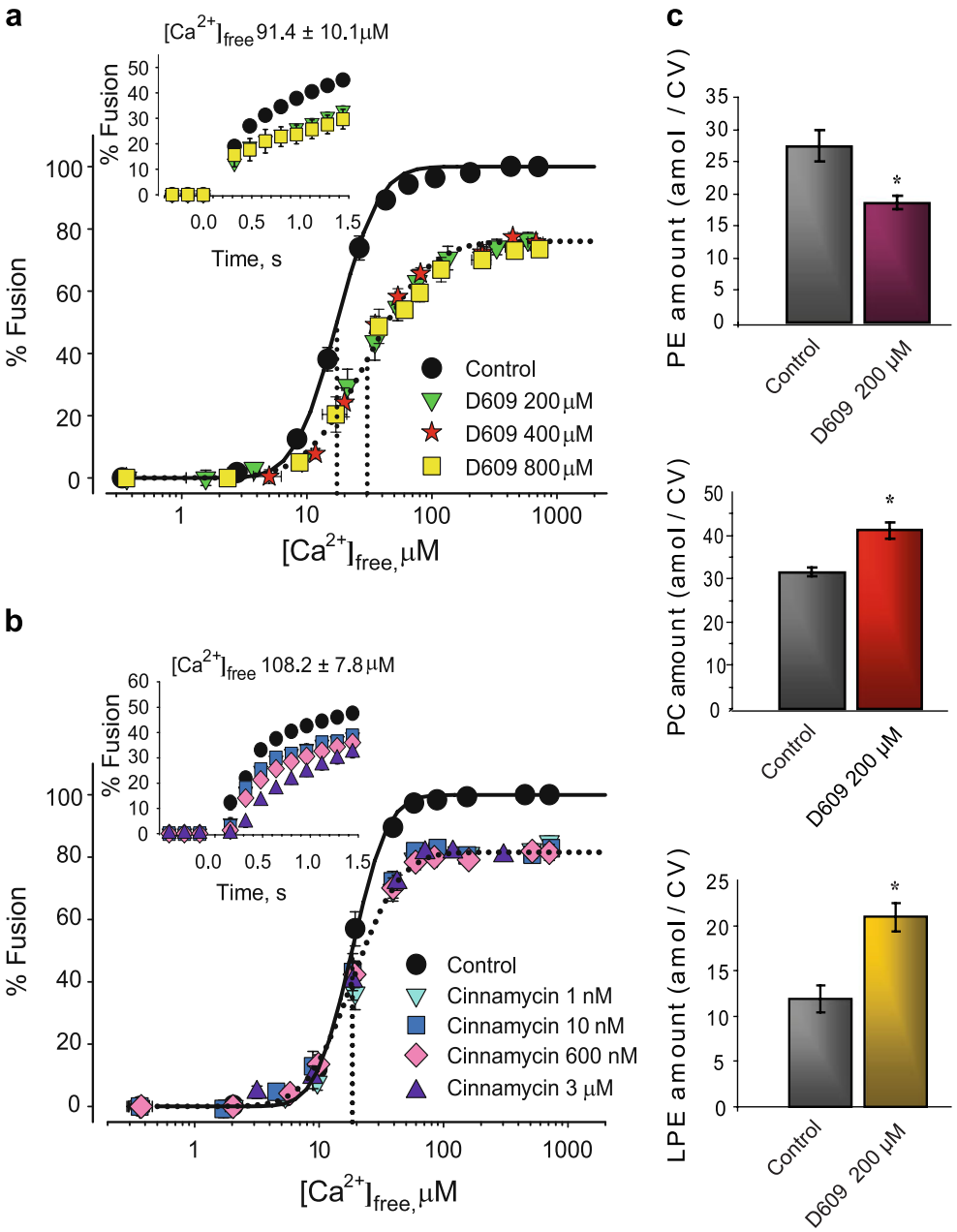

Fig. 6 PE depletion or sequestration inhibits CV–CV fusion. **a** Ca^{2+}–activity curves of CV from D609-treated eggs, including kinetics (*inset*) (n=3–6). *Vertical dotted lines* indicate EC_{50} of each curve. **b** Ca^{2+}–activity curves of cinnamycin-treated CV, including kinetics (*inset*) (n=3–5). *Vertical dotted lines* indicate EC_{50} of each curve. **c** Detection and quantification of CV membrane PC, PE and lysoPE following D609 treatments (n=4–5; representative image). *P<0.05 indicates significant difference from control

Cinnamycin also caused a dose-dependent inhibition of fusion kinetics (Fig. 6b). In response to 108.2±7.8 µM $[Ca^{2+}]_{free}$ initial fusion rate decreased by 23.2±1.5%/s and 44.6±0.6%/s with 1–600 nM and 3 µM cinnamycin, respectively. Notably, Ca^{2+} sensitivity was not affected. Lipid analyses showed no significant changes, confirming that cinnamycin binds to PE headgroups rather than extracting the lipid (not shown).

Considering the suggested roles of PIP species in exocytosis [5, 36, 59, 63], we studied their possible functions in Ca^{2+}-triggered fusion. Eggs were treated with Wrt and LY29 to down-regulate PI-3K activity. All fusion parameters were affected (Fig. 8a, b): 1 µM Wrt or 400 µM LY29 caused 29.6±3.0% and 23.1±3.4% inhibition of fusion extent, respectively; the EC_{50} right-shifted from 16.4±0.7 to 22.4±0.5 µM $[Ca^{2+}]_{free}$, and the initial fusion rate was inhibited by 38.2±3.3%/s and 41.7±2.5%/s, respectively (Fig. 8a, b). Comparable effects were seen in CV–PM fusion as well as in settle assays, confirming that inhibition was not associated with alterations in CV docking (Fig. 9a, b). However, LY29 has been reported to inactivate other kinases [64]. To test this, eggs were incubated with LY30, an ‘inactive’ analogue. One hundred and 200 µM LY30 had no effect on fusion parameters (Fig. 8c); LY29 was already inhibitory at these concentrations (Fig. 8a). At 400 µM, LY30 caused 15.0±2.9%

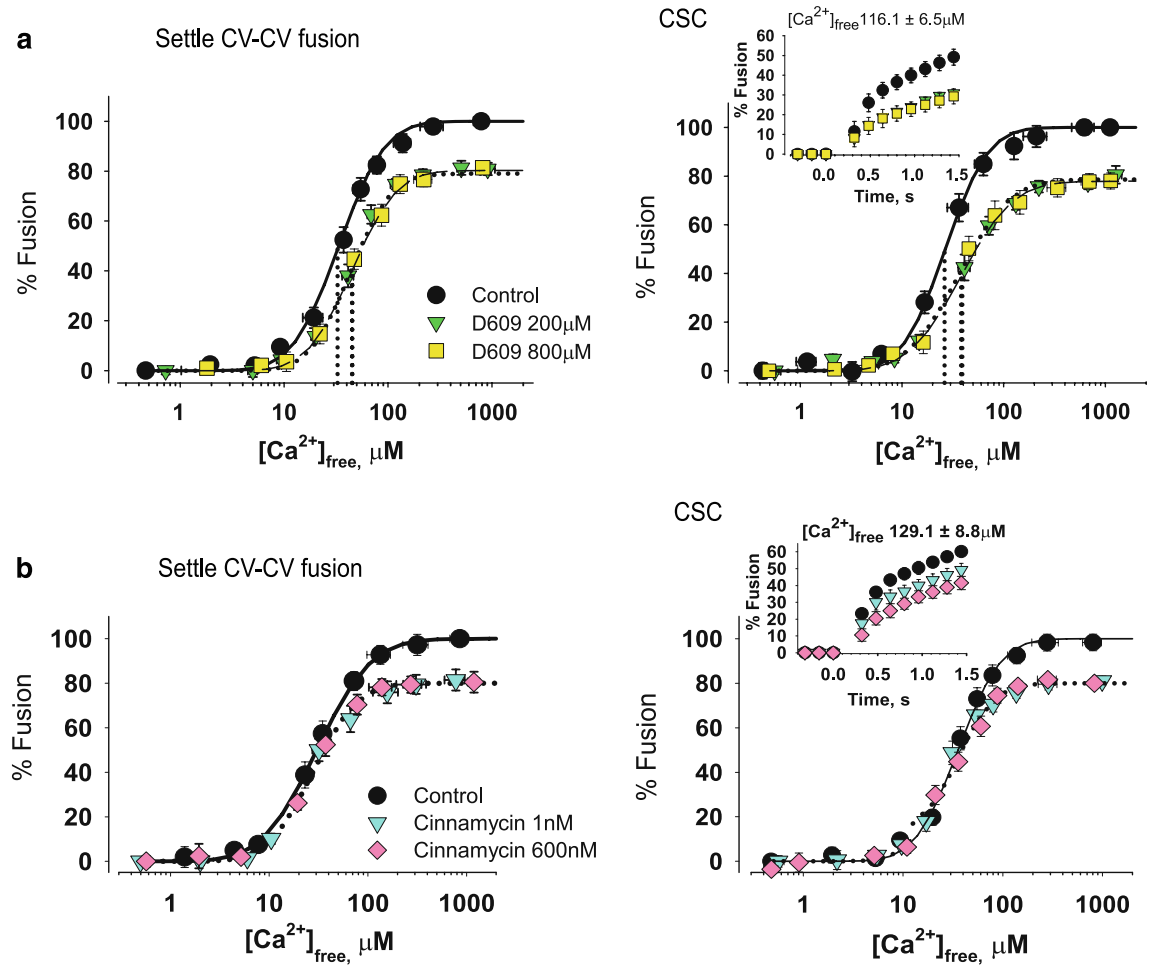

Fig. 7 PE depletion or sequestration inhibits CV–PM and settle CV–CV fusion. Ca^{2+}–activity curves of CV and CSC from D609-treated eggs (**a**), including kinetics (*inset*) (n=3–4) and cinnamycin-treated CV and CSC (**b**), including kinetics (*inset*) (n=3). *Vertical dotted lines* indicate EC_{50} of each curve

inhibition of fusion extent and 24.0±3.4%/s inhibition of initial rate. However, 400 μM LY30 had no effect on Ca^{2+} sensitivity, while 400 μM LY29 inhibited all fusion parameters, indicating that the effects of 100–200 μM LY29 (and partly 400 μM) are selective for PI-3K.

Molecular analyses of CV membranes indicated decreases in PI levels following egg incubations with Wrt and LY29 (Fig. 10a). CV membranes from Wrt-treated eggs (500 nM and 1 μM) had 15.2±1.2 and 14.9±0.9 amol/CV of PI, respectively, and from LY29-treated eggs (200 and 400 μM), CV membranes had 14.9±0.5 and 11.9±1.0 amol/CV of PI, respectively (vs. 19.8±1.0 amol/CV in controls), indicating that LY29 and Wrt have a similar capacity to decrease PI levels (Fig. 10a). Wrt and LY29 consistently enhanced PI(4)P levels relative to controls (1.55±0.08 amol/CV, Table 2). Following egg incubations with 500 nM and 1 μM Wrt, PI(4)P levels increased by 16.1% and 23.2%, respectively; LY29 treatments (200 and 400 μM) caused a 34.8% and 42.6% increase in PI(4)P, respectively (Fig. 10a). Controls had 2.86±0.25 and 1.22±0.08 amol/CV of PI(3,4)P2 and PI(3,4,5)P3, respectively (Table 2). PI(3,4,5)P3 decreased significantly following egg treatments with 1 μM Wrt (0.99±0.06 amol/CV), while LY29 had no effect (Fig. 10b). In contrast, CV from LY29-treated eggs had significantly lower PI(3,4)P2 levels (1.19±0.06 amol/CV), whereas Wrt had no significant effect (Fig. 10b). Despite the sensitivity of our detection protocols and lipid isolation from substantial amounts of CV membranes, concentrations of PI(3,5)P2 and PI(4,5)P2 could not be determined; detection limits indicated <1.03 and <1.71 amol/CV, respectively.

To block PIP, we treated CV and CSC with neomycin which has high affinity for PI/PIP, in particular PI(4,5)P2 [17, 40]. One hundred and 500 μM neomycin selectively inhibited fusion kinetics (by 30.4%/s, Figs. 8c and 9c). There were no changes in membrane lipids of neomycin-treated CV relative to controls (not shown), confirming that neomycin binds to PIP without extracting them.

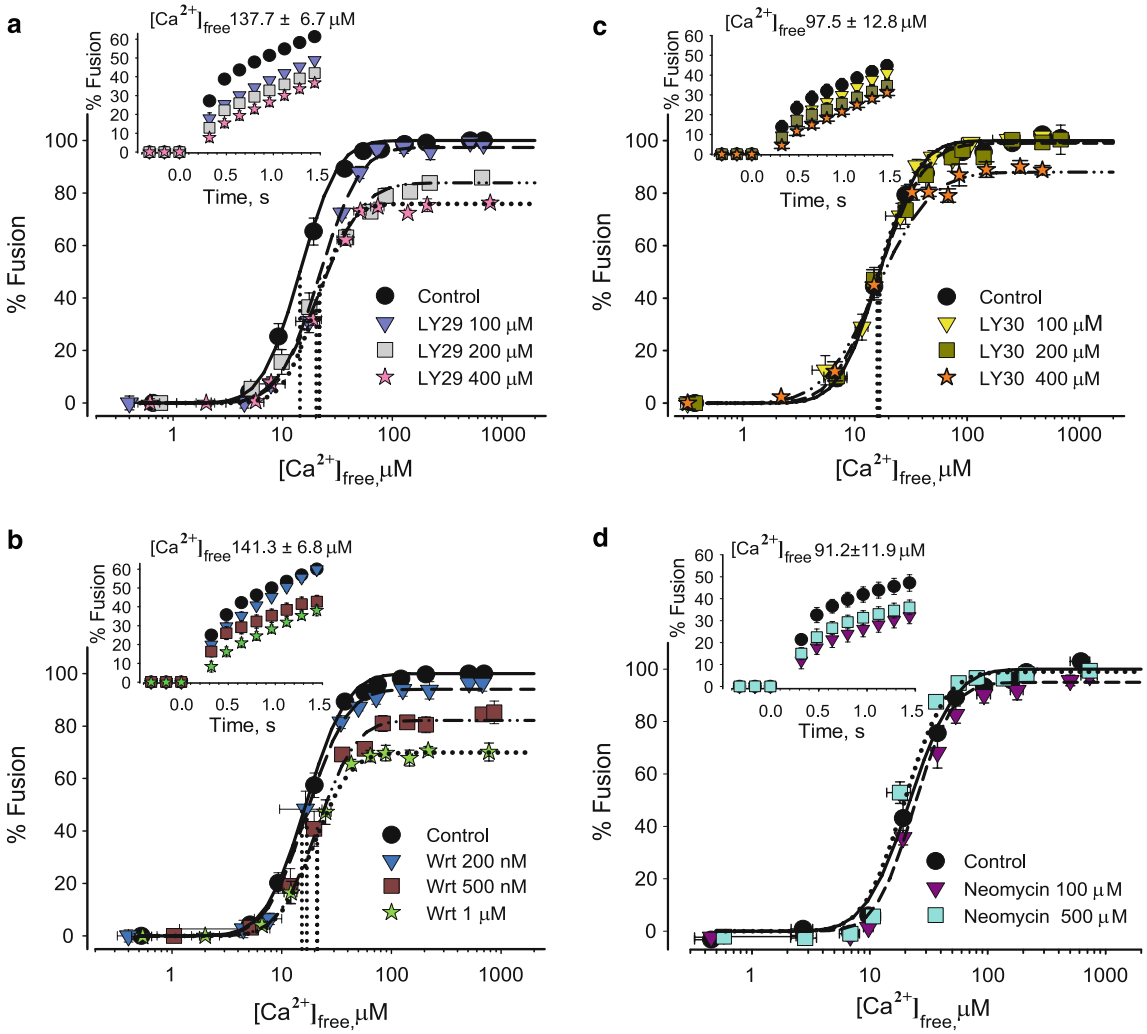

Fig. 8 PIP changes affect CV fusion. Ca^{2+}–activity curves of CV from eggs incubated with **a** LY29 (n=4), **b** Wrt (n=3–4), and **c** LY30 (n=3) including kinetics (*inset*). *Vertical dotted lines* indicate EC_{50} of each curve. **d** Ca^{2+}–activity curves of neomycin-treated CV (n=3–4) including kinetics (*inset*)

Discussion

Here we document a new analytical approach based on ex vivo egg manipulations with well-characterized pharmacological reagents that effect selective changes in the molecular composition of fully docked, primed, and release-ready CV, resulting in functional changes in fusion parameters. Using this approach that does not require direct physical manipulations of vesicle components, we demonstrate that:

- PIP play upstream roles in priming rather than directly in fusion; modulatory effects on kinetics are physiologically important, revealing more details concerning membrane domains defining the fusion site.
- Fully docked vesicles are subject to different priming states; PI-3K-dependent priming is likely the last necessary step to establish the fusion readiness of docked vesicles. Vesicles undergo priming/depriming steps without altering the fully docked state.
- PE has an essential role in membrane merger and a selective influence on fusion kinetics, likely contributing (with CHOL) to the composition of the necessary membrane domains.
- CHOL has a central role in the fusion mechanism, contributing a critical local negative curvature to promote native fusion and organizing microdomains to support fusion efficiency.

Ex vivo incubations target enzymatic pathways

To further promote analyses of the fusion mechanism, specific enzymatic pathways in unfertilized eggs were targeted with selective pharmacological reagents. We started by comparing freshly isolated and incubated eggs (Fig. 2). Proteomic analysis

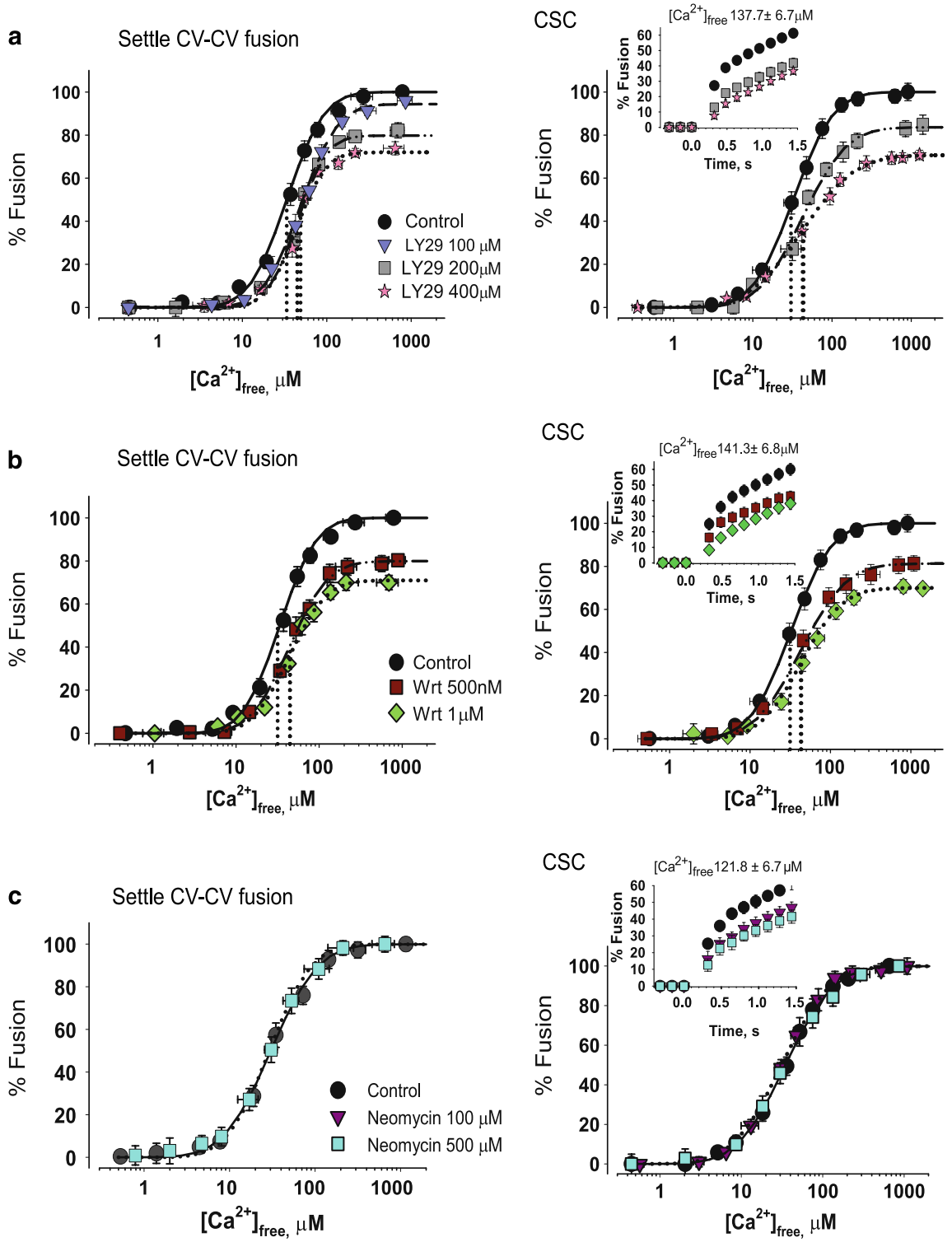

Fig. 9 Inhibition of PI-3K pathway or blockage of PI/PIP affects settle CV–CV and/or CV–PM fusion. Ca^{2+}–activity curves of CV and CSC from eggs incubated with **a** LY29 (n=3–4) and **b** Wrt (n=3), including kinetics (*inset*). *Vertical dotted lines* indicate EC_{50} of each curve. **c** Ca^{2+}–activity curves of neomycin-treated CV and CSC (n=2–3) including kinetics (*inset*)

identified some protein changes arising during incubations; nonetheless, these proteins cannot be key players in the fusion pathway as no detectable alterations in fusion parameters occurred. Similarly, incubations did not affect CV lipids.

To characterize essential and modulatory components involved in native membrane fusion, we targeted HMG-CoA reductase, squalene synthase, PLC, and PI-3K; for each, sequence analysis of sea urchin and human isoforms

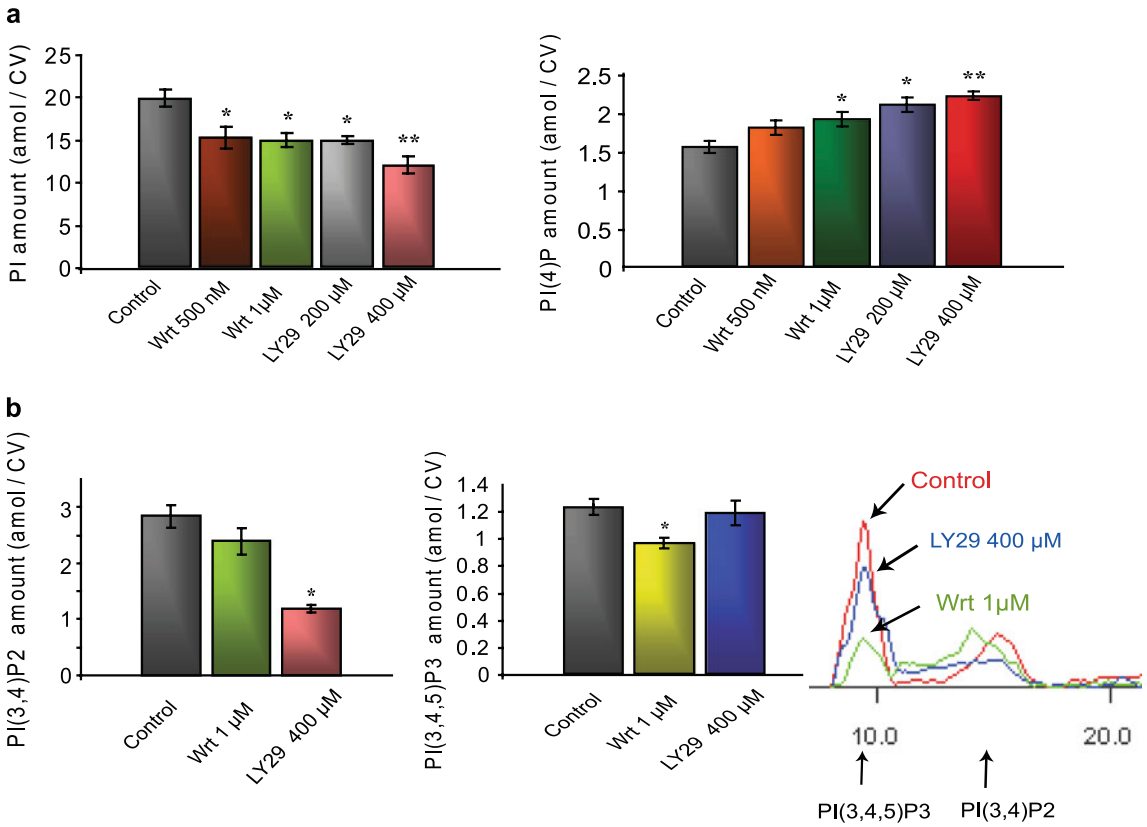

Fig. 10 LY29 and Wrt affect PIP levels in CV membranes. **a** Quantification of CV membrane PI and PI(4)P (n=5–8); *P<0.05, **P<0.05 indicate significant difference from control and other conditions, respectively. **b** Detection and quantification of CV membrane PI, PI(3,4)P2 and PI(3,4,5)P3 following treatments with LY29 (*blue line*, n=4–6) or Wrt (*green line*, n=6–8, representative image). *P<0.001 indicates significant difference from control for PI(3,4)P2 detected after LY29 treatments; *P<0.05 indicates significant difference from control for PI(3,4,5)P3 detected after Wrt treatments

revealed extensive homology, including catalytic domains (Table 3). DNA sequence analysis of HMG-CoA reductase cross-hybridizing regions indicated homology of the sea urchin protein (72%) with the carboxyl-terminal sequence of hamster HMG-CoA reductase [93]; human HMG-CoA reductase DNA also shares homology with this hamster reductase domain [54]. A conserved structure of all squalene synthases is an α-helical core surrounding an active site, containing signature 'aspartate-rich' sequences [2]; sea urchin squalene synthase has homology to known protein sequences, particularly in regions interacting with prenyl substrates [71]. Domains critical for PLC activity are found in urchin PLC: sea urchin PLC-δ contains Ser522, Lys438, Lys440, and Arg549 that are important for human PLC activity [19, 33]. Based on structural/functional studies of human and sea urchin PI-3K, domains involved in catalysis (phox homology (PX) and C2 domains) are quite similar and likely mediate similar protein–protein interactions and/or binding to membrane lipids [22, 73]. All targeted enzymes thus contain critical domains that have been conserved throughout subsequent evolution, implicating similar catalytic functions in echinoderms and vertebrates. This is not surprising considering the general high degree of genetic conservation between urchins and humans [67]. Thus, we were confident that the tested drugs would have selective effects [6, 44, 61, 94].

Critical roles for CHOL in triggered membrane fusion

Here we demonstrate the quality of enzymatic interventions by using CHOL-lowering agents to target HMG-CoA reductase and squalene synthase. Decreased CV membrane CHOL correlated with inhibition of fusion (Figs. 3 and 4); exogenous CHOL recovered fusion in CHOL-depleted CV (Fig. 5a–d). Considering differences in effects of Atst and Smst on fusion, they likely differentially affect CHOL biosynthesis. Upon administration, Atst is an active compound and yields metabolites that are as potent as the parent drug [52], whereas Smst must be hydrolyzed to an active form. Atst has a longer half-life (14 h) compared to Smst (1.9 h), suggesting that Atst blocks the enzyme active site longer [28], accounting for the potency of Atst and differences in the effects on fusion. As Atst and Smst suppress the supply of CHOL and other nonsterol products,

there may be other molecular alterations caused by statins, including inhibition of protein prenylation (i.e., G proteins) [1]. Isoprenoid pathways diverge from CHOL biosynthesis at the farnesyl-disphosphate branch-point. A squalene synthase inhibitor, Zara, blocks the first committed step in CHOL synthesis and should not adversely affect isoprenoid pathways. As CHOL reduction correlated with fusion inhibition, including pronounced inhibition of fusion efficiency, this suggests a more potent effect of Zara on the stability of CHOL-rich microdomains [25, 27, 72]. Overall, these data highlight critical roles for CHOL in membrane fusion rather than a more central role of isoprenoids. Moreover, such localized CHOL may be critical to multiple steps of the fusion pathway [82, 88].

The fundamental fusion mechanism (FFM) and the larger, integrated physiological fusion machine (PFM) are affected by membrane lipids [25]. The addition of exogenous high positive curvature lipids to interacting monolayers or removing endogenous high negative curvature lipids effectively inhibits formation of high curvature intermediates [20, 26, 27, 86]. The delivery of exogenous CHOL to CHOL-depleted CV (CHOL reduced to ~36 amol/CV) recovered CHOL to native levels (~46 amol/CV; Fig. 5c, d); thus, ~10 amol/CV of CHOL was necessary to rescue fusion. To confirm the critical negative curvature-promoting role of CHOL in the formation of fusion intermediates [18, 26, 27], we used a structurally dissimilar curvature analogue αT, which selectively recovered fusion extent in CHOL-depleted CV (Fig. 5a, b, e). Compared to recovery of all fusion parameters with exogenous CHOL, the lack of recovery of Ca^{2+} sensitivity and fusion kinetics with αT linked rescue of fusion efficiency to integrity/organization of CHOL-rich microdomains [27, 72]. As Smst is less disruptive (vs. Atst) to microdomain organization and components supporting physiological Ca^{2+} sensitivity, αT also supported a slight recovery of initial kinetics after Smst treatments. These results (Figs. 3, 4, and 5) are consistent with a dual role for CHOL in the fusion mechanism: (1) a physiological fusion site/PFM organizer, defining fusion efficiency; and (2) a negative curvature-promoting FFM component, defining the ability to fuse [21, 25–27, 72].

A critical role for PE in triggered membrane fusion

The data establish a selective role for endogenous PE in the FFM and identify a unique correlation between PE and fusion kinetics, suggesting a modulatory role in the PFM. Parallel changes in CV membrane PE, PC, and lysoPE correlated with saturation of fusion inhibition at the lowest D609 concentration tested (Fig. 6a, c), suggesting a critical albeit limited PLC activity in unfertilized eggs. Notably, although too low to measure directly, any reductions in diacylglycerol levels would also contribute to a lower overall (local) negative curvature and thus a reduced potential to fuse. Focusing here on the data at hand, we undertook two separate analyses to better assess the role of PE in fusion. First, we compared the ability of PE- and CHOL-depleted CV to fuse (Figs. 3, 4, 5, and 6). Following egg incubations with D609, fusion extent of PE-depleted CV was inhibited by 23.1±1.4%, comparable to 20.3±2.7% in CHOL-depleted CV (for 100 μM Atst- or 200 μM Smst-treated eggs). Based on CHOL and PE spontaneous negative curvatures ($-0.037/-0.044\,Å^{-1}$ and $-0.035\,Å^{-1}$, respectively) [18, 26], quantitative analyses of CV membrane CHOL and PE after statin and D609 treatments indicated negative curvature deficits of −0.46±0.05 amol $Å^{-1}$/CV (for CHOL) and −0.40±0.04 amol $Å^{-1}$/CV (for PE), consistent with the quantitative relationship between fusion extent and the negative curvature each lipid imparts to membranes [26, 27]. This is also consistent with the need for substantially less αT (~1.2 amol/CV) to selectively rescue fusion extent. As αT has ~2-fold higher negative curvature ($-0.073\,Å^{-1}$) [10] than does CHOL and has limited transbilayer mobility [78], and thus remains almost

Table 3 Conservation of critical enzymes from *S. purpuratus* to *Homo sapiens*

Enzyme name	Percent identities	Percent similarity
HMG-CoA reductase	58.0% (530/903)	72.0% (657/903)
Sterol-sensing domain (SSD)	68.4%	
HMG-CoA reductases family domain	68.6%	
Squalene synthase (urchin hypothetical protein LOC586013)	60.0% (246/404)	78.0% (319/404)
Squalene and phytoene synthases signature 1	93.8%	
Squalene and phytoene synthases signature 2	84.6%	
PLC	61.0% (736/1191)	76.0% (915/1191)
PH domain	38.0%	
C2 domain	44.4%	
PI-3 kinase (urchin hypothetical protein XP_001193595.1)	41.0% (460/1101)	60.0% (664/1101)
PI-3 and 4 kinases family domain	70.4%	
PX domain	42.7%	
C2 domain	57.8%	

exclusively in the outer membrane leaflet, proportionally less αT was required to effectively rescue the extent of fusion; certainly the correlation is not exact [26] but this likely reflects that CHOL is also complexed with/bound to certain proteins and lipids, so that the amount effectively capable of contributing negative curvature may be a bit lower than the total we measured. Thus, fusion recovery by enrichment of CHOL-depleted CV with CHOL and αT correlated well with the respective negative curvature contributions of these lipids. Considering this evidence for a direct role of PE, we carried out a second test to determine if the inhibition following D609 treatments is due to reduced PE. We treated CV with cinnamycin to block PE as a critical curvature component; this inhibited fusion extent and kinetics without affecting Ca^{2+} sensitivity (Figs. 6b and 7b). Based on 1:1 cinnamycin–PE binding ratio [55], 1 nM cinnamycin correlated to ~100% PE binding. The minimal cinnamycin concentration that nonetheless caused maximal inhibition corresponded to ~33 amol/CV of PE; analyses of untreated CV indicated 27.4+2.5 amol/CV of PE (Fig. 6c). Considering rapid PE flip-flop between inner/outer membrane leaflets [26, 56], ~50% of PE (~13.5 amol/CV) would be in the contacting monolayer; saturation of binding and inhibition of function was thus expected at 1 nM cinnamycin if PE is a critical fusion component. Similarly, D609 decreased PE by ~9 amol/CV, causing ~23% inhibition of fusion extent. Thus, PE plays a critical role in membrane merger by contributing local curvature stress comparable to CHOL [26].

Removing/blocking membrane PE also inhibited initial fusion kinetics. As efficiency parameters are linked to integrity of CHOL-rich microdomains [26, 27, 38, 72], yet PE does not actively support domain formation/stability, our data provide clues as to the physical nature of microdomains and the localized, functional domain composition at fusion sites [25]. Simply, (1) different negative curvature lipids may contribute to a given fusion site, and (2) highly localized and somewhat more fluid PE regions within the broader microdomain matrix may be critical to PFM/FFM (see [25], Fig. 3)—these areas (and thus global domain structure) would be stabilized by cinnamycin, preserving Ca^{2+} sensitivity, but PE molecules could no longer contribute their negative curvature to promote fusion.

The decline in Ca^{2+} sensitivity after D609 treatments likely results from increases in vesicle PC and lysoPE rather than in reduced PE levels. It seems that a decrease in lysoPE acylation is responsible for reduced PE levels (likely linked to PLC inhibition and thus reductions in available diacylglycerol species from PC; this seems reasonable as the PC increase is approximately equivalent to the lysoPE increase). Thus, in addition to a decrease in negative curvature species, neutral (PC) and positive curvature (lysoPE) species increase. Considering pronounced inhibition occurring when lysolipids are added to contacting monolayers of CHOL-depleted CV [27], it seems unlikely that endogenous lysoPE contributes to fusion inhibition. Furthermore, as cinnamycin (Figs. 6b and 7b) binds preferentially to PE rather than to lysoPE [55], fusion inhibition correlates closely with loss or blockade of PE. As D609 inhibited fusion, lysoPE is also unlikely to strongly promote fusion even if present in distal monolayers. If lysoPE is equally distributed between membrane monolayers, increased PC may contribute to the energy barrier of membrane merger. This explains reduced Ca^{2+} sensitivity after D609 treatments; stronger Ca^{2+} triggering can overcome this energy barrier. While this explanation does not consider potential lipid–protein interactions, it is fundamentally consistent with physical/chemical characteristics of the identified molecules and of the resulting functional alterations.

Roles for polyphosphoinositides in regulated release

PI-3K products function as ligands for protein targeting modules (pleckstrin homology (PH) and PX domains) [92]. Signaling proteins with PH domains accumulate at PI-3K activation sites by directly binding to PI(3,4)P2 and PI(3,4,5)P3 [14, 36]. PIP can play a role as localized membrane sites for protein recruitment [15]. Thus, PI-3K inhibition can dramatically affect protein localization (i.e., PFM). Some PIP-binding proteins help regulate the secretory pathway [46, 59]. A type IV P-type ATPase, required for flippase activity, is a PI(4)P effector [62], suggesting that increased PI(4)P levels (Fig. 10a) may enhance flippase activity resulting in an unfavorable local lipid environment to support fusion. CAPS, rabphilin, and Syt1 support exocytosis via interaction with PIP [53, 65, 79]. CAPS, a component of the synaptic vesicle priming machinery, maintains a fusion-competent vesicle pool for transmitter release [47]. Syt1 and rabphilin contain C2 domains, interacting with PI(4,5)P2 and PI(3,4,5)P3; although such interactions are suggested to mediate Ca^{2+}-triggered merger [23, 53], our data rule out a direct role for PIP in fusion.

Despite comparable effects on fusion, parallel egg incubations with LY29 and Wrt differentially affected PI(3,4)P2 and PI(3,4,5)P3 levels (none of these changes were linked to any effect on inter-membrane attachment, i.e., docking), emphasizing the importance of using more than one inhibitor in such studies (Fig. 10a, b). The 'inactive' analogue LY30 was tested here in parallel with PI-3K inhibitor LY29. As 400 μM LY30 inhibited fusion extent and kinetics (although Ca^{2+} sensitivity was not affected), this indicated that LY29 might have effects independent of PI-3K inhibition; alternately, at high concentrations, LY30 might also inhibit PI-3K (Fig. 8c). Nonetheless, as inhibition with LY30 was only

seen at 400 μM, using LY29 and Wrt in parallel provides valuable information concerning PIP roles in the FFM/PFM.

Considering the multiple roles suggested for PI(4,5)P2 in exocytotis/endocytotis, it is rather intriguing that its levels were well below detection limits (despite these limits being in the 1–2-amol/CV range). As CV are docked and fusion-ready, these low levels indicate that PI(4,5)P2 is either highly localized [4, 46, 83] to serve specific functions or not essential to the Ca^{2+}-triggered fusion step. If PI(4,5)P2 is generally found in PM, then these data suggest that PI (4,5)P2 is not critical to membrane merger per se (FFM). If PI(4,5)P2 supports upstream trafficking functions [36, 83], a role already fulfilled in release-ready CV, then its lower levels are expected. Similarly, if PI(4,5)P2 is critical in priming (our data do not support a role in inter-membrane attachment as docking was not affected), then it would have already served that function in release-ready CV; perhaps PI (4,5)P2 hydrolysis is actually the critical late priming step. In part, this may also link PI(4,5)P2 as an early substrate for diacylglycerol production [37] that may later function in the fusion reaction [26]. Thus, reduced PI(4,5)P2 levels are expected in vesicles at the fully docked, fusion-ready stage. In contrast, PI(4,5)P2 formation in the PM during or immediately after triggered release is critical for its subsequent roles in endocytosis [83, 89]. This suggests that PI(3,4)P2, PI(3,4,5)P3, and their immediate precursors PI(4)P and PI(4,5)P2 are not essential to docking/fusion steps per se and are not directly involved in the mechanism. An alternate interpretation is that the local ratio of specific PIP is critical; this ratio may be different for docking, priming, and maintenance of the primed state.

PI-3K products affect the activation of protein kinase-dependent pathways and can be associated with vesicle depriming [74]. It was shown that synapsin1-associated PI-3K regulates the size of the ready-releasable pool of synaptic vesicles [32]. Considering the essential role of PI-3K in ATP-dependent priming [59] and that PI-3K inhibitors can compete with PIP for the kinase ATP-binding site [81, 95], inhibition of fusion extent seen here (Figs. 8a, b and 9a, b) is likely caused by CV depriming in the fully docked state. Thus, changes are most consistent with isolation of a reduced pool of fusion-competent CV from LY29- and Wrt-treated eggs rather than with a direct role of PIP in triggered fusion. Reversible priming steps exist in the fully docked state; PI-3K activity seems likely to define the last necessary priming step in the docked state, consistent with earlier findings that only ~10% of docked neuroendocrine vesicles were fully release-ready, the remainder having to pass rapidly through a final preparatory step to confer fusion competence [66].

We used an additional test to establish if PIP changes directly influence fusion steps themselves by blocking CV membrane PIP with neomycin (Figs. 8d and 9c). At 10 mM, neomycin inhibited exocytosis in CSC preparations [40, 58]. Here, isolated CV provide direct access to the entire membrane, thereby enabling more selective concentrations of neomycin to be used; selective inhibition of kinetics (Figs. 8d and 9c) suggests dissociation of PIP from a direct role in fusion (i.e., FFM). As fusion efficiency is linked to integrity of CHOL-rich microdomains [27, 39, 72], comparable inhibition of fusion kinetics with LY29, Wrt, and neomycin suggests effects on the functional status/stability of such domains. Thus, changes in PIP may affect modulatory components, reorganizing and/or activating efficiency factors in the microdomain-associated PFM. Additionally, considering differences in PIP phosphorylation and therefore differences in total CV surface charge following LY29, Wrt, and neomycin treatments, and the fact that suppression of fusion was inconsistent with changes in more or less phosphorylated PIP, it appears unlikely that inter-membrane Ca^{2+} binding to negatively charged PIP headgroups plays any substantial role in fusion.

As a whole, the results tend to support roles for PIP in trafficking and priming that are already completed in this system (CV are docked and fusion-ready). Thus, PIP may potentially mediate a closer apposition of membranes by regulating the assembly or interactions of protein complexes as an important prelude to fusion and/or may also interact with CHOL-rich microdomains, affecting their inherent functions/stability [51, 83]. Our findings imply that PIP in concert with CHOL can be used by different fusion sites/PFMs to modulate the fusion process. In this light, different PIP (or ratios thereof) may have distinct functions, revealing more complex levels of regulation in triggering and achieving/maintaining fusion competence. The results suggest that a specific balance of these lipids is critical, raising the question of how PIP interact with CHOL, organizing PFM via CHOL-rich microdomains [25].

Concluding remarks

Taken together, the results highlight the essential roles for CHOL and PE in the mechanism of Ca^{2+}-triggered membrane fusion and provide new insights concerning possible modulatory roles for PIP. Although the data tend to rule out a direct role for PIP in membrane merger (FFM), they identify an important link with efficiency (PFM), particularly with regard to fusion rate. The involvement of key phosphoinositide, PE, and CHOL metabolism reactions in different disease states emphasizes the importance of this research [3, 7, 69]. Using selective pharmacological interventions at specific steps of metabolic pathways, this new ex vivo approach enables effective and meaningful molecular alterations that aid further dissection of fundamental priming, docking, and membrane fusion mechanisms. Coupled with quantitative

fusion assays and well-established acute manipulations of CV membrane composition, this approach is a robust high-throughput platform to definitively identify specific molecular components of the Ca^{2+}-triggered steps of regulated exocytosis.

Acknowledgments The authors acknowledge the support of the Natural Sciences and Engineering Research Council of Canada (NSERC), the Canadian Institutes of Health Research (CIHR), and the University of Western Sydney. The authors thank Drs. M.A. Churchward and K. Furber for helpful discussions and D. Bininda for assistance with aquatics.

References

1. Alaei P, MacNulty EE, Ryder NS (1996) Inhibition of protein prenylation down-regulates signalling by inflammatory mediators in human keratinocytes. Biochem Biophys Res Commun 222:133–138
2. Ashby MN, Edwards PA (1990) Elucidation of the deficiency in two yeast coenzyme Q mutants. Characterization of the structural gene encoding hexaprenyl pyrophosphate synthetase. J Biol Chem 265:13157–13164
3. Bader AG, Kang S, Zhao L, Vogt PK (2005) Oncogenic PI3K deregulates transcription and translation. Nat Rev Cancer 5:921–929
4. Bai J, Tucker WC, Chapman ER (2004) PIP2 increases the speed of response of synaptotagmin and steers its membrane-penetration activity toward the plasma membrane. Nat Struct Mol Biol 11:36–44
5. Begle A, Tryoen-Toth P, de BJ B, MF VN (2009) ARF6 regulates the synthesis of fusogenic lipids for calcium-regulated exocytosis in neuroendocrine cells. J Biol Chem 284:4836–4845
6. Bergstrom JD, Dufresne C, Bills GF, Nallin-Omstead M, Byrne K (1995) Discovery, biosynthesis, and mechanism of action of the zaragozic acids: potent inhibitors of squalene synthase. Annu Rev Microbiol 49:607–639
7. Berman DE, Dall'Armi C, Voronov SV, McIntire LB, Zhang H, Moore AZ, Staniszewski A, Arancio O, Kim TW, Di PG (2008) Oligomeric amyloid-beta peptide disrupts phosphatidylinositol-4, 5-bisphosphate metabolism. Nat Neurosci 11:547–554
8. Blank PS, Cho MS, Vogel SS, Kaplan D, Kang A, Malley J, Zimmerberg J (1998) Submaximal responses in calcium-triggered exocytosis are explained by differences in the calcium sensitivity of individual secretory vesicles. J Gen Physiol 112:559–567
9. Bligh E, Dyer W (1959) A rapid method of total lipid extraction and purification. Can J Biochem Physiol 37:911–917
10. Bradford A, Atkinson J, Fuller N, Rand RP (2003) The effect of vitamin E on the structure of membrane lipid assemblies. J Lipid Res 44:1940–1945
11. Brown MS, Goldstein JL (1980) Multivalent feedback regulation of HMG CoA reductase, a control mechanism coordinating isoprenoid synthesis and cell growth. J Lipid Res 21:505–517
12. Butt RH, Coorssen JR (2005) Postfractionation for enhanced proteomic analyses: routine electrophoretic methods increase the resolution of standard 2D-PAGE. J Proteome Res 4:982–991
13. Butt RH, Lee MW, Pirshahid SA, Backlund PS, Wood S, Coorssen JR (2006) An initial proteomic analysis of human preterm labor: placental membranes. J Proteome Res 5:3161–3172
14. Cantley LC (2002) The phosphoinositide 3-kinase pathway. Science 296:1655–1657
15. Carlton JG, Cullen PJ (2005) Coincidence detection in phosphoinositide signaling. Trends Cell Biol 15:540–547
16. Chandler DE (1984) Exocytosis involves highly localized membrane fusions. Biochem Soc Trans 12:961–963
17. Chen Q, Boss WF (1991) Neomycin inhibits the phosphatidylinositol monophosphate and phosphatidylinositol bisphosphate stimulation of plasma membrane ATPase activity. Plant Physiol 96:340–343
18. Chen Z, Rand RP (1997) The influence of cholesterol on phospholipid membrane curvature and bending elasticity. Biophys J 73:267–276
19. Cheng HF, Jiang MJ, Chen CL, Liu SM, Wong LP, Lomasney JW, King K (1995) Cloning and identification of amino acid residues of human phospholipase C delta 1 essential for catalysis. J Biol Chem 270:5495–5505
20. Chernomordik L, Chanturiya A, Green J, Zimmerberg J (1995) The hemifusion intermediate and its conversion to complete fusion: regulation by membrane composition. Biophys J 69:922–929
21. Chernomordik L, Kozlov MM, Zimmerberg J (1995) Lipids in biological membrane fusion. J Membr Biol 146:1–14
22. Cho W, Stahelin RV (2006) Membrane binding and subcellular targeting of C2 domains. Biochim Biophys Acta 1761:838–849
23. Chung SH, Song WJ, Kim K, Bednarski JJ, Chen J, Prestwich GD, Holz RW (1998) The C2 domains of Rabphilin3A specifically bind phosphatidylinositol 4, 5-bisphosphate containing vesicles in a Ca2+-dependent manner. In vitro characteristics and possible significance. J Biol Chem 273:10240–10248
24. Churchward MA, Brandman DM, Rogasevskaia T, Coorssen JR (2008) Copper (II) sulfate charring for high sensitivity on-plate fluorescent detection of lipids and sterols: quantitative analyses of the composition of functional secretory vesicles. J Chem Biol 1:79–87
25. Churchward MA, Coorssen JR (2009) Cholesterol, regulated exocytosis, and the physiological fusion. Biochem J 423:1–14
26. Churchward MA, Rogasevskaia T, Brandman DM, Khosravani H, Nava P, Atkinson JK, Coorssen JR (2008) Specific lipids supply critical negative spontaneous curvature—an essential component of native Ca2+-triggered membrane fusion. Biophys J 94:3976–3986
27. Churchward MA, Rogasevskaia T, Hofgen J, Bau J, Coorssen JR (2005) Cholesterol facilitates the native mechanism of Ca2+-triggered membrane fusion. J Cell Sci 118:4833–4848
28. Conde K, Roy S, Freake HC, Newton RS, Fernandez ML (1999) Atorvastatin and simvastatin have distinct effects on hydroxy methylglutaryl-CoA reductase activity and mRNA abundance in the guinea pig. Lipids 34:1327–1332
29. Coorssen JR, Blank PS, Albertorio F, Bezrukov L, Kolosova I, Backlund PS Jr, Zimmerberg J (2002) Quantitative femto- to attomole immunodetection of regulated secretory vesicle proteins critical to exocytosis. Anal Biochem 307:54–62
30. Coorssen JR, Blank PS, Albertorio F, Bezrukov L, Kolosova I, Chen X, Backlund PS Jr, Zimmerberg J (2003) Regulated secretion: SNARE density, vesicle fusion and calcium dependence. J Cell Sci 116:2087–2097
31. Coorssen JR, Blank PS, Tahara M, Zimmerberg J (1998) Biochemical and functional studies of cortical vesicle fusion: the SNARE complex and Ca2+ sensitivity. J Cell Biol 143:1845–1857
32. Cousin MA, Malladi CS, Tan TC, Raymond CR, Smillie KJ, Robinson PJ (2003) Synapsin I-associated phosphatidylinositol 3-kinase mediates synaptic vesicle delivery to the readily releasable pool. J Biol Chem 278:29065–29071
33. Coward K, Owen H, Poustka AJ, Hibbitt O, Tunwell R, Kubota H, Swann K, Parrington J (2004) Cloning of a novel phospholipase C-delta isoform from pacific purple sea urchin (*Strongylocentrotus purpuratus*) gametes and its expression during early embryonic development. Biochem Biophys Res Commun 313:894–901
34. Crossley I, Swann K, Chambers E, Whitaker M (1988) Activation of sea urchin eggs by inositol phosphates is independent of external calcium. Biochem J 252:257–262

35. Decker SJ, Kinsey WH (1983) Characterization of cortical secretory vesicles from the sea urchin egg. Dev Biol 96:37–45
36. Di PG, De CP (2006) Phosphoinositides in cell regulation and membrane dynamics. Nature 443:651–657
37. Dumas F, Byrne RD, Vincent B, Hobday TM, Poccia DL, Larijani B (2010) Spatial regulation of membrane fusion controlled by modification of phosphoinositides. PLoS ONE 5(8):e12208
38. Furber KL, Brandman DM, Coorssen JR (2009) Enhancement of the Ca(2+)-triggering steps of native membrane fusion via thiol-reactivity. J Chem Biol 2:27–37
39. Furber KL, Churchward MA, Rogasevskaia TP, Coorssen JR (2009b) Identifying critical components of native Ca2+-triggered membrane fusion. Integrating studies of proteins and lipids. Ann N Y Acad Sci 1152:121–134
40. Gabev E, Kasianowicz J, Abbott T, McLaughlin S (1989) Binding of neomycin to phosphatidylinositol 4, 5-bisphosphate (PIP2). Biochim Biophys Acta 979:105–112
41. Haggerty JG, Jackson RC (1983) Release of granule contents from sea urchin egg cortices. New assay procedures and inhibition by sulfhydryl-modifying reagents. J Biol Chem 258:1819–1825
42. Hao M, Lin SX, Karylowski OJ, Wustner D, McGraw TE, Maxfield FR (2002) Vesicular and non-vesicular sterol transport in living cells. The endocytic recycling compartment is a major sterol storage organelle. J Biol Chem 277:609–617
43. Hibbert JE, Butt RH, Coorssen JR (2006) Actin is not an essential component in the mechanism of calcium-triggered vesicle fusion. Int J Biochem Cell Biol 38:461–471
44. Houle S, Marceau F (2003) Wortmannin alters the intracellular trafficking of the bradykinin B2 receptor: role of phosphoinositide 3-kinase and Rab5. Biochem J 375:151–158
45. Hwang R, Lee EJ, Kim MH, Li SZ, Jin YJ, Rhee Y, Kim YM, Lim SK (2004) Calcyclin, a Ca2+ ion-binding protein, contributes to the anabolic effects of simvastatin on bone. J Biol Chem 279:21239–21247
46. James DJ, Khodthong C, Kowalchyk JA, Martin TF (2008) Phosphatidylinositol 4, 5-bisphosphate regulates SNARE-dependent membrane fusion. J Cell Biol 182:355–366
47. Jockusch WJ, Speidel D, Sigler A, Sorensen JB, Varoqueaux F, Rhee JS, Brose N (2007) CAPS-1 and CAPS-2 are essential synaptic vesicle priming proteins. Cell 131:796–808
48. Jury EC, Isenberg DA, Mauri C, Ehrenstein MR (2006) Atorvastatin restores Lck expression and lipid raft-associated signaling in T cells from patients with systemic lupus erythematosus. J Immunol 177:7416–7422
49. Knight DE, Scrutton MC (1986) Gaining access to the cytosol: the technique and some applications of electropermeabilization. Biochem J 234:497–506
50. Konig S, Hoffmann M, Mosblech A, Heilmann I (2008) Determination of content and fatty acid composition of unlabeled phosphoinositide species by thin-layer chromatography and gas chromatography. Anal Biochem 378:197–201
51. Krauss M, Haucke V (2007) Phosphoinositides: regulators of membrane traffic and protein function. FEBS Lett 581:2105–2111
52. Lea AP, McTavish D (1997) Atorvastatin. A review of its pharmacology and therapeutic potential in the management of hyperlipidaemias. Drugs 53:828–847
53. Loyet KM, Kowalchyk JA, Chaudhary A, Chen J, Prestwich GD, Martin TF (1998) Specific binding of phosphatidylinositol 4, 5-bisphosphate to calcium-dependent activator protein for secretion (CAPS), a potential phosphoinositide effector protein for regulated exocytosis. J Biol Chem 273:8337–8343
54. Luskey KL, Stevens B (1985) Human 3-hydroxy-3-methylglutaryl coenzyme A reductase. Conserved domains responsible for catalytic activity and sterol-regulated degradation. J Biol Chem 260:10271–10277
55. Machaidze G, Seelig J (2003) Specific binding of cinnamycin (Ro 09-0198) to phosphatidylethanolamine. Comparison between micellar and membrane environments. Biochemistry 42:12570–12576
56. Marx U, Lassmann G, Holzhutter HG, Wustner D, Muller P, Hohlig A, Kubelt J, Herrmann A (2000) Rapid flip-flop of phospholipids in endoplasmic reticulum membranes studied by a stopped-flow approach. Biophys J 78:2628–2640
57. Matese JC, McClay DR (1998) Cortical granule exocytosis is triggered by different thresholds of calcium during fertilisation in sea urchin eggs. Zygote 6(55–64):65a
58. McLaughlin S, Whitaker M (1988) Cations that alter surface potentials of lipid bilayers increase the calcium requirement for exocytosis in sea urchin eggs. J Physiol 396:189–204
59. Meunier FA, Osborne SL, Hammond GR, Cooke FT, Parker PJ, Domin J, Schiavo G (2005) Phosphatidylinositol 3-kinase C2alpha is essential for ATP-dependent priming of neurosecretory granule exocytosis. Mol Biol Cell 16:4841–4851
60. Muller-Decker K (1989) Interruption of TPA-induced signals by an antiviral and antitumoral xanthate compound: inhibition of a phospholipase C-type reaction. Biochem Biophys Res Commun 162:198–205
61. Murdock DK, Murdock AK, Murdock RW, Olson KJ, Frane AM, Kersten ME, Joyce DM, Gantner SE (1999) Long-term safety and efficacy of combination gemfibrozil and HMG-CoA reductase inhibitors for the treatment of mixed lipid disorders. Am Heart J 138:151–155
62. Natarajan P, Liu K, Patil DV, Sciorra VA, Jackson CL, Graham TR (2009) Regulation of a Golgi flippase by phosphoinositides and an ArfGEF. Nat Cell Biol 11:1421–1426
63. Oberdorf J, Vilar-Rojas C, Epel D (1989) The localization of PI and PIP kinase activities in the sea urchin egg and their modulation following fertilization. Dev Biol 131:236–242
64. Okkenhaug K, Vanhaesebroeck B (2001) New responsibilities for the PI3K regulatory subunit p85 alpha. Sci STKE 2001(65):pe1
65. Osborne SL, Wen PJ, Meunier FA (2006) Phosphoinositide regulation of neuroexocytosis: adding to the complexity. J Neurochem 98:336–342
66. Parsons TD, Coorssen JR, Horstmann H, Almers W (1995) Docked granules, the exocytic burst, and the need for ATP hydrolysis in endocrine cells. Neuron 15:1085–1096
67. Pennisi E (2006) Genetics. Sea urchin genome confirms kinship to humans and other vertebrates. Science 314:908–909
68. Pettitt TR, Dove SK, Lubben A, Calaminus SD, Wakelam MJ (2006) Analysis of intact phosphoinositides in biological samples. J Lipid Res 47:1588–1596
69. Puglielli L, Friedlich AL, Setchell KD, Nagano S, Opazo C, Cherny RA, Barnham KJ, Wade JD, Melov S, Kovacs DM, Bush AI (2005) Alzheimer disease beta-amyloid activity mimics cholesterol oxidase. J Clin Invest 115:2556–2563
70. Racchi M, Baetta R, Salvietti N, Ianna P, Franceschini G, Paoletti R, Fumagalli R, Govoni S, Trabucchi M, Soma M (1997) Secretory processing of amyloid precursor protein is inhibited by increase in cellular cholesterol content. Biochem J 322(Pt 3):893–898
71. Robinson GW, Tsay YH, Kienzle BK, Smith-Monroy CA, Bishop RW (1993) Conservation between human and fungal squalene synthetases: similarities in structure, function, and regulation. Mol Cell Biol 13:2706–2717
72. Rogasevskaia T, Coorssen JR (2006) Sphingomyelin-enriched microdomains define the efficiency of native Ca(2+)-triggered membrane fusion. J Cell Sci 119:2688–2694
73. Seet LF, Hong W (2006) The Phox (PX) domain proteins and membrane traffic. Biochim Biophys Acta 1761:878–896
74. Storz P, Toker A (2002) 3′-Phosphoinositide-dependent kinase-1 (PDK-1) in PI 3-kinase signaling. Front Biosci 7:d886–d902

75. Stricker SA (1999) Comparative biology of calcium signaling during fertilization and egg activation in animals. Dev Biol 211:157–176
76. Szule JA, Coorssen JR (2003) Revisiting the role of SNAREs in exocytosis and membrane fusion. Biochim Biophys Acta 1641:121–135
77. Tanimoto T, Ohya S, Tsujita Y (1998) Inhibitory activity to protein prenylation and antifungal activity of zaragozic acid D3, a potent inhibitor of squalene synthase produced by the fungus, *Mollisia* sp. SANK 10294. J AntibiotTokyo 51:428–431
78. Tiurin VA, Kagan VE, Serbinova EA, Gorbunov NV, Erin AN (1986) The interaction of alpha-tocopherol with phospholipid liposomes: the absence of transbilayer mobility. Biull Eksp Biol Med 102:689–692
79. Tucker WC, Weber T, Chapman ER (2004) Reconstitution of Ca2+-regulated membrane fusion by synaptotagmin and SNAREs. Science 304:435–438
80. Vacquier VD (1975) The isolation of intact cortical granules from sea urchin eggs: calcium ions trigger granule discharge. Dev Biol 43:62–74
81. Vanhaesebroeck B, Leevers SJ, Ahmadi K, Timms J, Katso R, Driscoll PC, Woscholski R, Parker PJ, Waterfield MD (2001) Synthesis and function of 3-phosphorylated inositol lipids. Annu Rev Biochem 70:535–602
82. Vardjan N, Stenovec M, Jorgacevski J, Kreft M, Zorec R (2007) Subnanometer fusion pores in spontaneous exocytosis of peptidergic vesicles. J Neurosci 27:4737–4746
83. Vicinanza M, D'Angelo G, Di CA, De Matteis MA (2008) Phosphoinositides as regulators of membrane trafficking in health and disease. Cell Mol Life Sci 65:2833–2841
84. Vogel SS, Blank PS, Zimmerberg J (1996) Poisson-distributed active fusion complexes underlie the control of the rate and extent of exocytosis by calcium. J Cell Biol 134:329–338
85. Vogel SS, Delaney K, Zimmerberg J (1991) The sea urchin cortical reaction. A model system for studying the final steps of calcium-triggered vesicle fusion. Ann N Y Acad Sci 635:35–44
86. Vogel SS, Leikina EA, Chernomordik LV (1993) Lysophosphatidylcholine reversibly arrests exocytosis and viral fusion at a stage between triggering and membrane merger. J Biol Chem 268:25764–25768
87. Vogel SS, Zimmerberg J (1992) Proteins on exocytic vesicles mediate calcium-triggered fusion. Proc Natl Acad Sci U S A 89:4749–4753
88. Wang N, Kwan C, Gong X, de Chaves EP, Tse A, Tse FW (2010) Influence of cholesterol on catecholamine release from the fusion pore of large dense core chromaffin granules. J Neurosci 30:3904–3911
89. Wenk MR, De CP (2004) Protein–lipid interactions and phosphoinositide metabolism in membrane traffic: insights from vesicle recycling in nerve terminals. Proc Natl Acad Sci U S A 101:8262–8269
90. Wessel GM, Brooks JM, Green E, Haley S, Voronina E, Wong J, Zaydfudim V, Conner S (2001) The biology of cortical granules. Int Rev Cytol 209:117–206
91. Wipf P, Halter RJ (2005) Chemistry and biology of wortmannin. Org Biomol Chem 3:2053–2061
92. Wishart MJ, Dixon JE (2002) PTEN and myotubularin phosphatases: from 3-phosphoinositide dephosphorylation to disease. Trends Cell Biol 12:579–585
93. Woodward HD, Allen JM, Lennarz WJ (1988) 3-Hydroxy-3-methylglutaryl coenzyme A reductase in the sea urchin embryo is developmentally regulated. J Biol Chem 263:2513–2517
94. Wu ZL, O'Kane TM, Connors TJ, Marino MJ, Schaffhauser H (2008) The phosphatidylinositol 3-kinase inhibitor LY 294002 inhibits GlyT1-mediated glycine uptake. Brain Res 1227:42–51
95. Wymann MP, Bulgarelli-Leva G, Zvelebil MJ, Pirola L, Vanhaesebroeck B, Waterfield MD, Panayotou G (1996) Wortmannin inactivates phosphoinositide 3-kinase by covalent modification of Lys-802, a residue involved in the phosphate transfer reaction. Mol Cell Biol 16:1722–1733
96. Zimmerberg J, Blank PS, Kolosova I, Cho MS, Tahara M, Coorssen JR (2000) A stage-specific preparation to study the Ca(2+)-triggered fusion steps of exocytosis: rationale and perspectives. Biochimie 82:303–314
97. Zimmerberg J, Coorssen JR, Vogel SS, Blank PS (1999) Sea urchin egg preparations as systems for the study of calcium-triggered exocytosis. J Physiol 520(Pt 1):15–21
98. Zimmerberg J, Sardet C, Epel D (1985) Exocytosis of sea urchin egg cortical vesicles in vitro is retarded by hyperosmotic sucrose: kinetics of fusion monitored by quantitative light-scattering microscopy. J Cell Biol 101:2398–2410